Nano Materials Science 3 (2021) 344–367

Contents lists available at ScienceDirect

Nano Materials Science

journal homepage: www.keaipublishing.com/cn/journals/nano-materials-science/

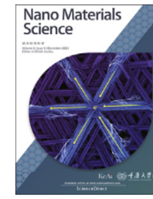

Photoelectrocatalytic carbon dioxide reduction: Fundamental, advances and challenges

Peng Chen [a,b], Yuxin Zhang [c], Ying Zhou [a], Fan Dong [a,b,*]

[a] *School of New Energy and Materials, Southwest Petroleum University, Chengdu, 610500, China*
[b] *Research Center for Environmental and Energy Catalysis, Institute of Fundamental and Frontier Sciences, University of Electronic Science and Technology of China, Chengdu, 611731, China*
[c] *College of Materials Science and Engineering, Chongqing University, Chongqing, 400044, China*

ARTICLE INFO

Keywords:
Photoeletrocatalytic
CO_2 reduction
Basic principles
Influencing factors
Reaction mechanisms

ABSTRACT

With the rising global population, increasing energy demand and rapid climate change, great concerns have been raised for environment and energy security in future. Solar-driven CO_2 reduction provides a promising way to deal with energy crisis and global warming, which has been widely concerned. Photoelectrocatalysis technology can effectively utilize solar energy and avoid to use high-temperature and high-voltage reduction environment by integrating the vantages of both photocatalysis and electrocatalysis, which exhibits a broad application prospect of CO_2 reduction with a high efficiency and excellent selectivity. In this review, basic principles of CO_2 reduction by photocatalysis, electrocatalysis and photoeletrocatalysis are briefly reviewed, also comparing the technical characteristics of the above technologies. Different photoelectrocatalytic systems for CO_2 reduction are described and compared. The several key influencing factors of photoelectrocatalytic performance of CO_2 reduction are discussed, including interaction between reaction molecules and catalysts, reaction conditions and influence of photoelectrode. Then, the advances on reaction mechanisms and strategies of performance enhancement by optimizing photoexcitation, charge separation efficiency and surface reaction were reviewed. Besides, the challenges and prospects of photoelectrocatalytic CO_2 reduction will be also discussed.

1. Introduction

With the increase of global population, energy demand and climate change, great concerns have been raised for future energy security. Energy consumption mainly comes from the combustion of fossil fuels such as coal, oil, and natural gas, which also releases excessive carbon dioxide (CO_2) into atmosphere and thus exacerbates greenhouse effect to cause global warming [1–3]. Converting atmospheric CO_2 into low-carbon fuels or small-molecule organic compounds not only benefits CO_2 emission reduction, but also can be used as a carrier of energy storage, which exhibits great significance to alleviate energy shortage and global environmental pollution [4–7].

At present, the artificial methods for CO_2 conversion mainly include high-temperature catalytic hydrogenation, electrocatalytic reduction, photocatalytic conversion and photoelectrocatalytic methods [8–11]. For the CO_2 reduction by high-temperature catalytic hydrogenation, the process must input high energy and hydrogen sources that is usually provided by the combustion of fossil fuels. Therefore, such conversion itself will cause the energy consumption and the generation of more CO_2 [12]. Due to the sufficient electrons in the electrocatalytic reduction, which will simultaneously realize the multi electron reduction process, resulting in a variety of products. Additionally, the different reduction medium (gas phase or liquid phase) and reaction temperature (high or low temperature) will further lead to the increase of product types. If the external voltage is too high, it will also lead to the competitive reaction of hydrogen evolution, resulting in the reduction of Faraday efficiency in the process of electrocatalytic reduction. In addition, the type of electrode or catalyst and the magnitude of external voltage lead to the fact that the electrocatalytic reduction does not have absolute selectivity for a product (usually a mixture of several substances), which is a grand challenge for electrocatalytic reduction of CO_2 [13,14]. Contrast to above technologies, photocatalytic CO_2 reduction can effectively utilize the solar energy and avoid the use of high-temperature and high-voltage reduction environment, which has a broad application prospect.

* Corresponding author. School of New Energy and Materials, Southwest Petroleum University, Chengdu, 610500, China.
E-mail addresses: dfctbu@126.com, dongfan@uestc.edu.cn (F. Dong).

https://doi.org/10.1016/j.nanoms.2021.05.003
Received 20 March 2021; Accepted 25 April 2021
Available online 1 June 2021

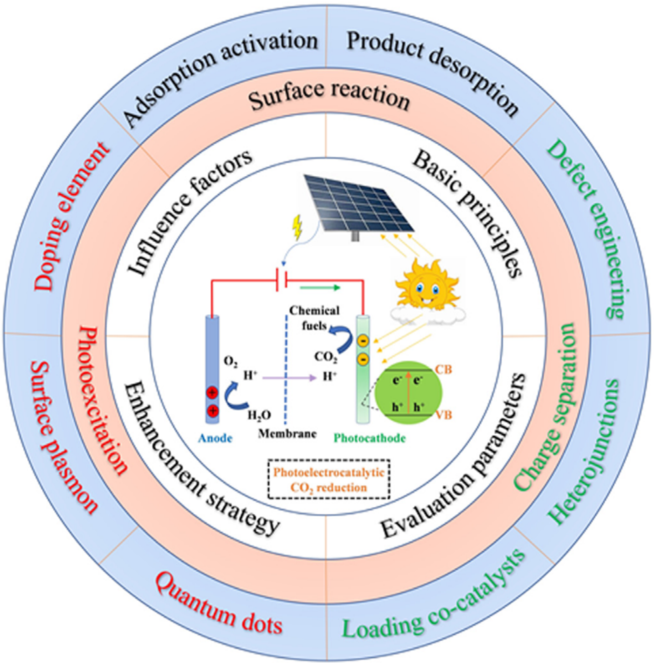

Scheme 1. The whole framework of this review.

However, photocatalysts generally exist limited utilization efficiency of solar energy and low separation efficiency of photogenerated carrier, which leads to the low efficiency of photocatalytic CO_2 reduction. Besides, abundant sacrificial agents are often added in the liquid-solid photocatalytic system of CO_2 reduction, leading to the increase of economic cost. Additionally, the current catalytic efficiency is relatively low in the gas-solid photocatalytic system of CO_2 reduction. Therefore, the practical application of current photocatalytic CO_2 reduction technology is restricted [11,15,16]. Considering those problems, the researchers put forward the technology of photoelectrocatalytic CO_2 reduction by integrating the characteristics of photocatalysis and electrocatalysis. Photoeletrocatalytic system can promote the carrier separation by adjusting overpotential and also realize the quick transfer of multi electrons and protons, which results in improving catalytic reaction efficiency to rapidly obtain the products of CO_2 reduction on the cathode. And product selectivity can be tuned by optimizing the main reaction steps of photoelectrocatalytic CO_2 reduction process on cathode. Moreover, photoelectrocatalysis can overcome the energy barrier owing to insufficient redox potential by using external voltage, realizing higher solar conversion efficiency compared with photocatalysis [11,17–19]. These excellent characteristics make the technology of photoelectrocatalytic CO_2 reduction show great application potential.

In this review (Scheme 1), basic principles of CO_2 reduction by photocatalysis, electrocatalysis and photoelectrocatalysis will be briefly reviewed. The several key influencing factors of photoelectrocatalytic performance are discussed, including interaction between reaction molecules and catalysts (initial activation and C–C bond formation), reaction conditions (such as light source, electrolyte effect and overpotential, etc.) and influence of photoelectrode (thermodynamics and kinetics). The advances on the design of photoeletrocatalytic materials, reaction mechanisms, influence factors and strategies of performance enhancement will be comprehensively reviewed. The main strategies of enhancing product activity and selectivity on photoelectrode for CO_2 reduction are proposed, including photoexcitation (e.g., doping element, introducing surface plasmon and quantum dots), charge separation efficiency (e.g., loading co-catalysts, constructing heterojunction and defect structure), surface reaction (e.g., adsorption and activation of reactants, adsorption/desorption of intermediates), and their synergistic effects.

2. Basic principles of catalytic CO_2 reduction

2.1. Photocatalytic CO_2 reduction

The most common CO_2 conversion method is photosynthesis in natural world, which means that green plants or photosynthetic bacteria convert CO_2 in the air into oxygen and/or energy materials necessary for growth under light conditions. Photocatalytic (PC) reduction of CO_2 is similar to plant photosynthesis in Fig. 1a [20,21], which is that the electrons and holes on surface of photocatalyst respectively reduce CO_2 and oxidized water to produce oxygen under light irradiation. When the incident light energy is larger than the band gap (Eg), the electrons would be excited to conduction band (CB) while holes will be generated in valence band (VB), as shown in Fig. 1a. On the one hand, the photogenerated electrons and holes would recombine (volume recombination and surface recombination). On the other hand, the photogenerated electrons react with CO_2 adsorbed on the surface to generate CO, CH_4 and CH_3OH, etc., while photogenerated holes oxidize water to H^+ and O_2 [15,16,22,23].

Over the years, researchers have developed and designed many types of photocatalysts, including metal oxides [24–29], metal chalcogenides [30,31], metal nitrides [32], metal phosphides [33], layered double hydroxides (LDHs) [34] and non-metal semiconductors [35–37], etc. Although there are various photocatalytic materials, their practical application efficiency of CO_2 reduction is still not ideal. Therefore, researchers developed plentiful strategies of catalyst modification to optimize photocatalytic performance, including morphology and size control [38,39], crystal face control [40], doping [41,42], noble metal deposition [43,44], semiconductor recombination [45], dye sensitization [46], and defect construction [47,48], etc. To some extent, these modification strategies can improve efficiency of light utilization and carrier separation, thus enhancing the reactivity and product selectivity. However, a series of problems still exist in the practical application. For examples, many sacrificial agents usually need to be added in liquid-solid reaction system of photocatalytic CO_2 reduction that leads to increase the cost, while the catalytic efficiency is relatively low in the gas-solid reaction system, which further restricts the application of this technology. Therefore, it is necessary to develop new photocatalysts or new CO_2 reduction systems. Additionally, the studies about surface reaction process, absorption mechanism of solar energy, separation and migration of electrons/holes, are all conducive to elucidation of the surface microstructure and energy band structure of the catalyst, so as to improve the catalytic efficiency of CO_2 reduction [7,49–51].

2.2. Electrocatalytic CO_2 reduction

The process of electrocatalytic (EC) CO_2 reduction is that using external electric field as the main energy source to induce redox reaction on electrodes (Fig. 1b). The H_2O is oxidized to produce oxygen and protons on anode. And the protons migrate to participate in CO_2 reduction on cathode through proton exchange membrane. The reaction process of electrocatalytic CO_2 reduction is controllable by adjusting voltage and reaction condition. Due to the sufficient electron source in the electrocatalytic reduction, it will simultaneously realize the multi electron reduction process, resulting in a variety of products [13,14]. It should be noted that if the external voltage is too high, it will also lead to the competitive reaction of hydrogen evolution, which will lead to the reduction of Faraday efficiency of electrocatalytic CO_2 reduction. Moreover, the type of electrode or catalyst and the magnitude of external voltage would lead to the fact that the electrocatalytic reduction does not have absolute selectivity for a product, which usually includes a mixture of several substances. Therefore, one of the main challenges is to improve product selectivity of electrocatalytic CO_2 reduction by optimizing the electrode or catalyst. At present, the technology of electrocatalytic CO_2 reduction is still not mature enough due to the obstacles such as low energy efficiency, poor reaction selectivity and total conversion rate [13,

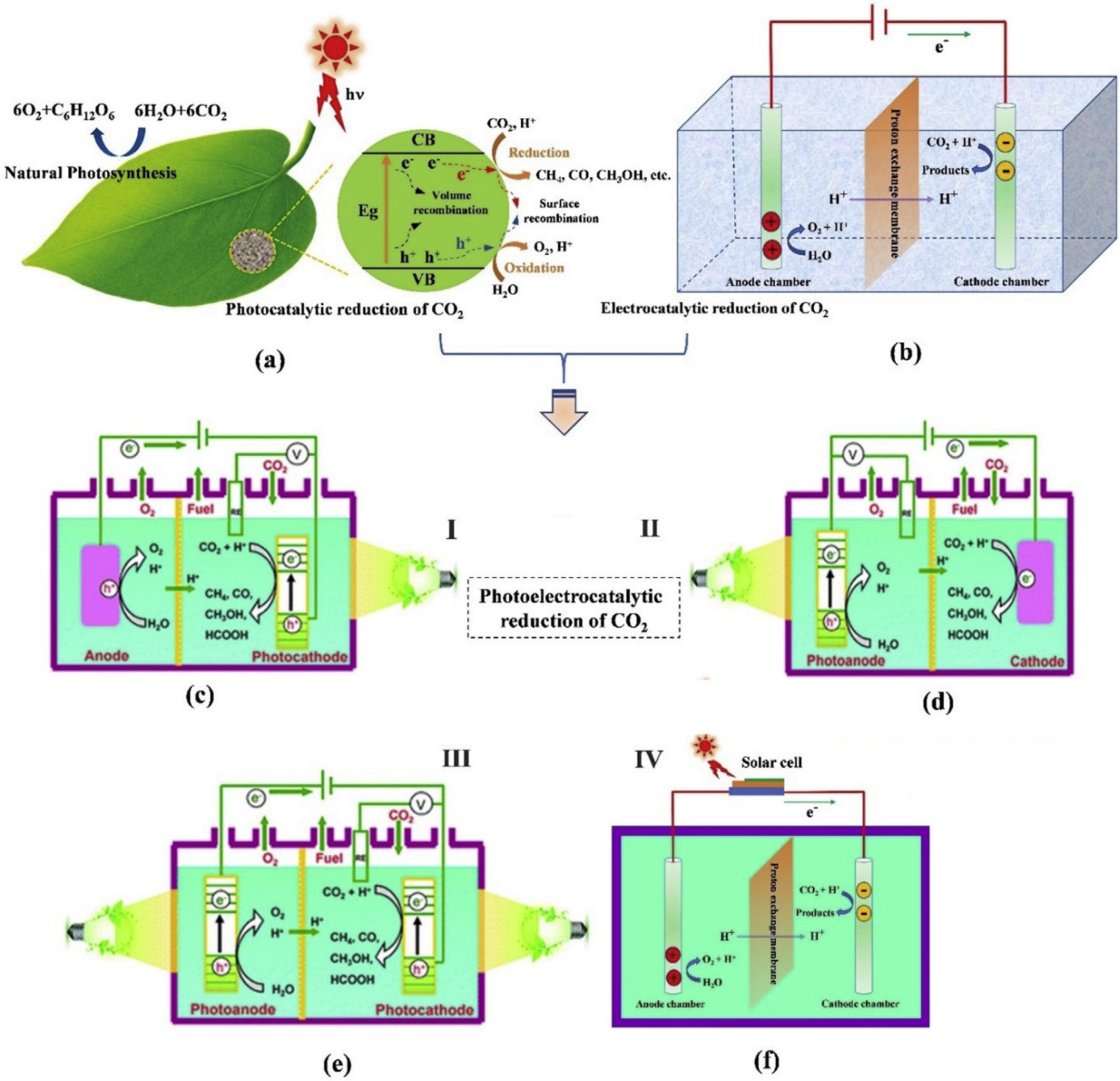

Fig. 1. Basic principles of catalytic CO_2 reduction. (a) Analogy diagram of natural photosynthesis and schematic of photocatalytic CO_2 reduction [20]. Reproduced with permission: Copyright 2017, American Chemical Society. (b) Schematic diagrams for electrocatalytic CO_2 reduction system. **Photoelectrocatalytic systems:** (c) photocathode + dark anode, (d) dark cathode + photoanode, (e) photocathode + photoanode [58], Reproduced with permission: Copyright 2016, Royal Society of Chemistry. (f) solar cell + electrodes.

14,52–54]. Birdja et al. points out that the systematic understanding of the intricate interaction among initial activation of CO_2, formation of C–C bond, surface structure, electrolyte effect and mass transfer is still insufficient [13]. In addition to focusing on the design of catalysts, researchers should also recognize the importance of electrode surface structure, reaction and process conditions. Therefore, combining with theory calculation and *in-situ* electrochemistry technology is necessary to develop more rigorous experiments and standardized procedures, to have a deeper understanding of the electrocatalysis on the catalyst surface, and to develop multi-scale calculation and modeling methods [13,49,55–57].

2.3. Main systems and principle of photoelectrocatalytic CO_2 reduction

Due to the limitation of photocatalytic and electrocatalytic CO_2 reduction in practical application, the researchers combined the two technologies to develop photoelectrocatalytic (PEC) reduction of CO_2. The photoelectrocatalytic CO_2 reduction refers to the process that the semiconductor photoelectrode generates electrons by photoexcitation, and then the electrons migrate to the electrode surface under the guidance of external voltage to carry out the catalytic reduction of CO_2 [59–62]. The action of external electric field is helpful to promote the directional transfer of photogenerated electrons and holes, and thus enhancing the separation efficiency of photogenerated carriers to greatly improve the redox ability. Simultaneously, when the band position of photocatalyst is not conducive to CO_2 reduction and H_2O oxidation, the redox potentials can be adjusted by applying appropriate bias voltage in the photoreduction system [17]. Compared to photocatalytic CO_2 reduction process, photoelectrocatalysis can realize the rapid transfer of electrons to reduce CO_2 on the photocathode at a lower overpotential, greatly enhancing reduction efficiency. Compared with single electrocatalysis, photoeletrocatalysis can use sunlight as the energy source to excite the generation of carriers, then participates in the oxidation-reduction reaction to finally realize the CO_2 reduction with low energy consumption. The whole process can reduce the input of

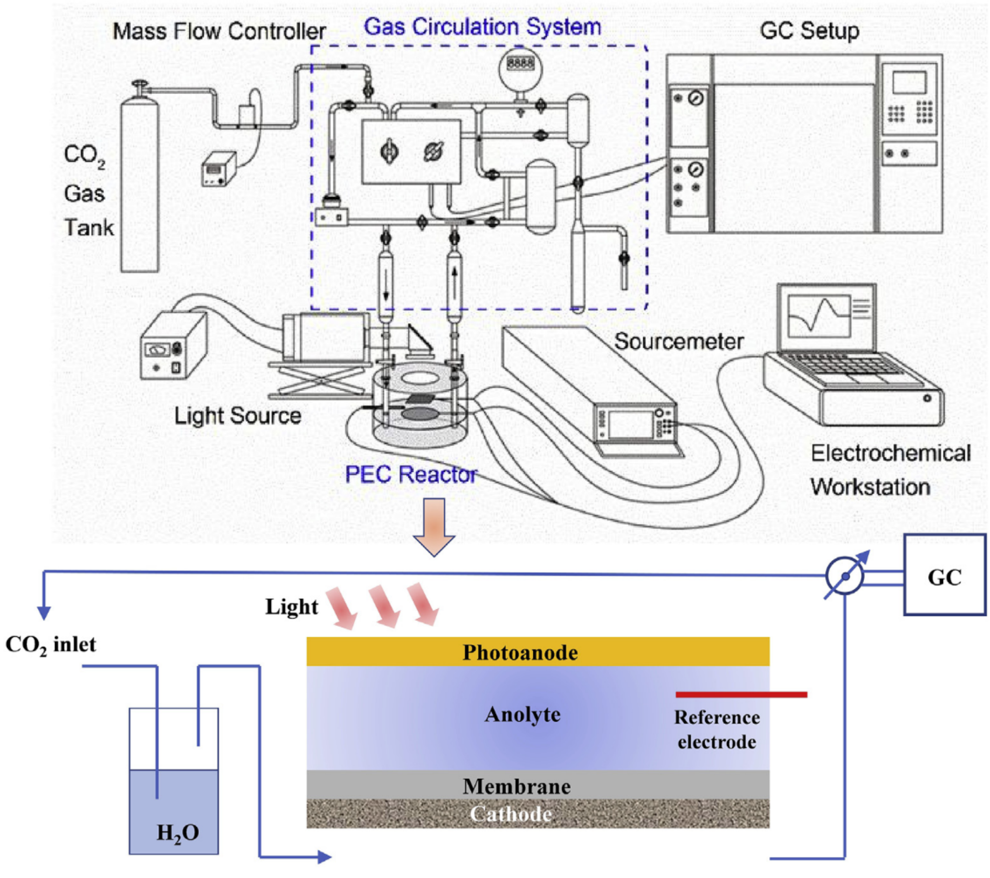

Fig. 2. Continuous-flow PEC CO_2 reduction system [81]. Reproduced with permission: Copyright 2020, American Chemical Society.

external energy and realize the utilization of low-carbon clean and sustainable energy. The excellent photoelectrocatalytic CO_2 reduction system can not only use photocatalysis activity to excite and generate carriers under light conditions, effectively reducing the energy input of external electrons and energy consumption, but also use electrocatalytic activity to improve the electron-hole separation and transmission, greatly enhancing reduction efficiency.

Most experiments of photoelectrocatalytic CO_2 reduction are mostly conducted in a three-electrode system including working electrode, counter electrode and reference electrode respectively. According to the different semiconductor materials of photoelectrode, the CO_2 reduction system can be divided into following categories (Fig. 1c–e): I. dark anode and *p*-type photocathode, II. dark cathode and *n*-type photoanode, III. *p*-type photocathode and *n*-type photoanode [58,63–66]. The *p*-type semiconductor photocathode not only works as a center of generating electrons and holes but also need to act as the catalyst for CO_2 activation to carry out reduction reaction. Generally, the *p*-type semiconductor photocathodes have negative CBs which are favorable for CO_2 reduction. But VB potentials of most *p*-type semiconductor are insufficient to oxidize water, which needs a higher bias potential generally to excite the reaction [58,67]. Additionally, H_2 is usually generated with CO and HCOOH on *p*-type semiconductor photocathodes, affecting the selectivity of CO_2 reduction. The frequently-used *p*-type materials as photocathode including *p*-GaP, *p*-InP, *p*-Cu_2O, *p*-CuO and *p*-CdTe, but which are generally expensive, toxic and/or unstable in aqueous solutions [68–71]. Instead, the most *n*-type semiconductors (e.g., TiO_2, WO_3, ZnO, Fe_2O_3, and $BiVO_4$) that made of earth-abundant elements are generally low-toxic or nontoxic and/or also highly stable in aqueous solutions [72–74]. Which makes the system (dark cathode and *n*-type photoanode) would be an attractive alternative. Furthermore, the combination of appropriate *p*-type and *n*-type semiconductors with matched band structure respectively as photocathode and photoanode to form Z-scheme heterojunction can realize efficient CO_2 reduction without external voltage [17,58]. However, it is worth noting that not all of this kind PEC CO_2 reduction systems can avoid bias voltage. For instance, the system composed of an *n*-type TiO_2 photoanode and a *p*-type Si photocathode was still needed a bias voltage to promote CO_2 reduction [75]. Additionally, a novel tandem device is developed by integrating a solar cell for supplying external voltage to promote CO_2 reduction reaction (Fig. 1f), also showing the excellent efficiency and promising potential [76–78]. When the external bias voltage generated by the solar cell is high enough, the system can realize the unassisted CO_2 reduction and avoid the strict conditions that needs to form Z-scheme heterojunction. Recently, some researchers considered the challenges of CO_2 conversion in traditional aqueous solution such as serious mass transfer limitation stemmed from low solubility and slow diffusion of raw material CO_2 in water [79,80], developing a continuous-flow system for PEC CO_2 reduction by direct introduction of gas CO_2 onto the surface of catalysts [81–84], as shown in Fig. 2. This new system shows an obvious advantage is that no limitations in CO_2 concentration exist due to solubility and diffusion through the double layer and competitive chemisorption of water is largely reduced [81,82].

3. Evaluation parameters for photoelectrocatalytic CO_2 reduction

The evaluation parameters for photocatalysis and electrocatalysis can combine to assess photoeletrocatalytic CO_2 reduction, as shown in Fig. 3 [61]. Which mainly include product conversion rate, catalytic current density, turnover number (TON), turnover frequency (TOF), quantum

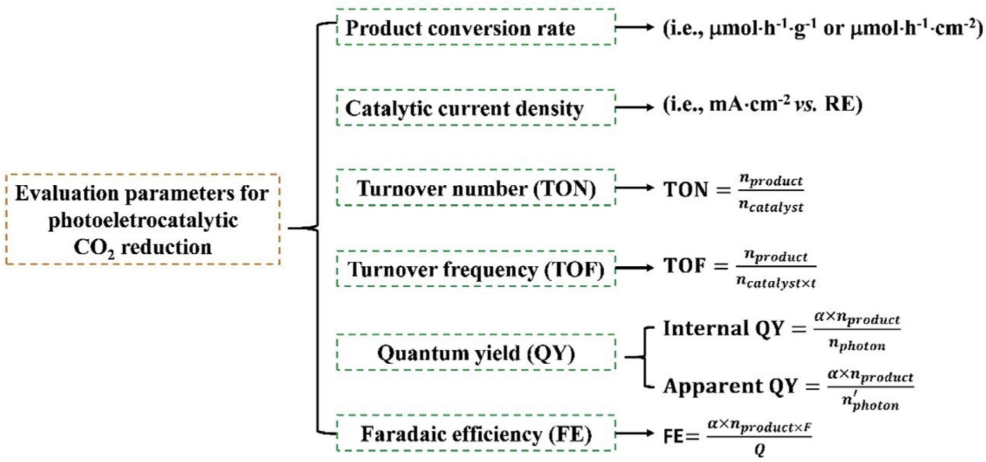

Fig. 3. Schematic diagram of evaluation parameters for photoelectrocatalytic CO_2 reduction. Where t represents the reaction time, $n_{product}$ and $n_{catalyst}$ respectively refer to molar numbers of products and photo-electrocatalysts. The α is the needed electron numbers for products. For examples, α is 2 when generated CO and α is 8 when generated CH_4. And n_{photon} and n'_{photon} are respectively the number of absorbed and incident photons. F and Q is the Faraday's constant and the total passed charge, respectively.

yield (QY) and Faradaic efficiency (FE). The product conversion rate is generally calculated the yield per hour of per unit mass or per unit area on photoelectrode. The catalytic current density is also an important index to evaluate the reaction efficiency, which needs to be compared with the reference electrode (RE). TON and TOF can reflect the activity of catalytic active centers. The utilization and conversion efficiency of solar energy can be evaluated by calculating the QY. Additionally, the product selectivity can be assessed by calculating FE.

4. Influence factors of photoelectrocatalytic CO_2 reduction

The influence factors of photoelectrocatalytic CO_2 reduction should be considered comprehensively from two aspects of photocatalysis and electrocatalysis [13,85–87]. Fig. 4 summarizes the main influencing factors of photoelectrocatalytic reduction of carbon dioxide, including influence of photoelectrode (thermodynamics and kinetics), interaction between reaction molecules and catalysts (initial activation and C–C bond formation), reaction conditions (such as light source, electrolyte effect and overpotential, etc.).

4.1. Thermodynamics and kinetics on photoelectrode

Photoelectrocatalytic CO_2 reduction belongs to complex multistep reactions, intrinsic properties of semiconductor photoelectrode can influence the reduction efficiency and product selectivity [87]. Firstly, the critical start step is to produce electrons and holes in semiconductor photoelectrode by photoexcitation. The energy of light absorption determines whether the semiconductor can be excited and how many electron-hole pairs can be generated, which affects reaction rate and product selectivity of CO_2 reduction from thermodynamic. Significantly, the different reduction potentials will determine the specific products in CO_2 reduction. Photogenerated electrons need sufficient reduction ability to trigger a specific reduction reaction in thermodynamics, thus affecting the product selectivity of CO_2 reduction. The reduction ability of photogenerated electron is correlated with the CB position of semiconductor photoelectrode. Fig. 4a outlines the correlation between standard redox potential of various products and the positions of CB and VB in some typical semiconductors. The effective electron-hole separation can increase the electron density on the surface of the photoelectrode, which can dynamically increase reaction rate and obtain higher reduction state products. In addition, the interaction between reactants and surface catalytic active sites can directly affect multi-step reaction of CO_2 reduction, thus determining the product selectivity. Exploring the relationship between the dynamic changes of surface active sites and the reaction efficiency is the key to achieve accurate control of CO_2 reduction [88]. Moreover, the adsorption/desorption of reactants/intermediates can affect the exposure of active sites and the reaction rate on the surface photoelectrode, which will also determine the product selectivity from kinetics [87,89–92].

4.2. Interaction between molecules and catalysts

4.2.1. Initial activation of CO_2 molecules

The activation of CO_2 molecule is first step in photoelectrocatalytic CO_2 reduction. In general, the activation and reduction of CO_2 is difficult owing to the negative reduction potential of forming the $CO_2\bullet^-$ radical intermediate by first electron transferring and because CO_2 is a very stable molecule [93]. A less negative reduction potentials can be induced via forming chemical bonds between CO_2 and suitable photo-electrocatalysts, thus stabilizing $CO_2\bullet^-$ radicals or intermediates. Therefore, selecting the right catalyst can directly reduce CO_2 to two-electron products (CO or HCOOH) at low overpotential [94–96]. Birdja et al. [13] considered four reduction processes related to CO_2 activation (Eqs. (1) - (4)):

$$* + CO_2 + H^+ + e^- \rightarrow *COOH \quad (1)$$

$$* + CO_2 + H^+ + e^- \rightarrow *OCHO \quad (2)$$

$$* + CO_2 + e^- \rightarrow *CO_2^- \quad (3)$$

$$* + H^+ + 2e^- \rightarrow *H^- \quad (4)$$

Considering the simultaneous transfer of protons and electrons, the initial activation of CO_2 can be deduced according to equations (1) and (2), and four possible bonding modes were shown in Fig. 4b, which are called concerted proton–electron transfer (CPET) reactions [97]. Whether *COOH or *OCHO is the first intermediate of generating CO or HCOOH still remains controversial. By calculating the binding energy, it is found that post-transition metals (e.g., Pb and Sn) are more likely to combine CO_2 through oxygen and have selectivity for formic acid, while transition metal electrodes are more likely to combine CO_2 through carbon [97]. When the initial activation of CO_2 involves only one-electron transfer, the binding step of CO_2 can be deduced via equation (3). If the formation of $*CO_2^-$ is rate determining step, the product selectivity is strongly influenced by the pH value [98].Additionally, equation (4) shows the formation of anionic hydride on the surface of catalyst. The Rh, Sn and In protoporphyrins can reduce CO_2 to formic acid with a high selectivity, and the main reason is that the formation of the key intermediate (anionic hydride) to attack C atom of CO_2 according to density functional theory (DFT) results [99,100]. The steps involved in equations (3) and (4) called sequential proton–electron transfer (SPET), Fig. 4b exhibits a summary of the discussed activation mechanisms for CO_2 reduction [13]. Compared with the formed intermediates in CPET,

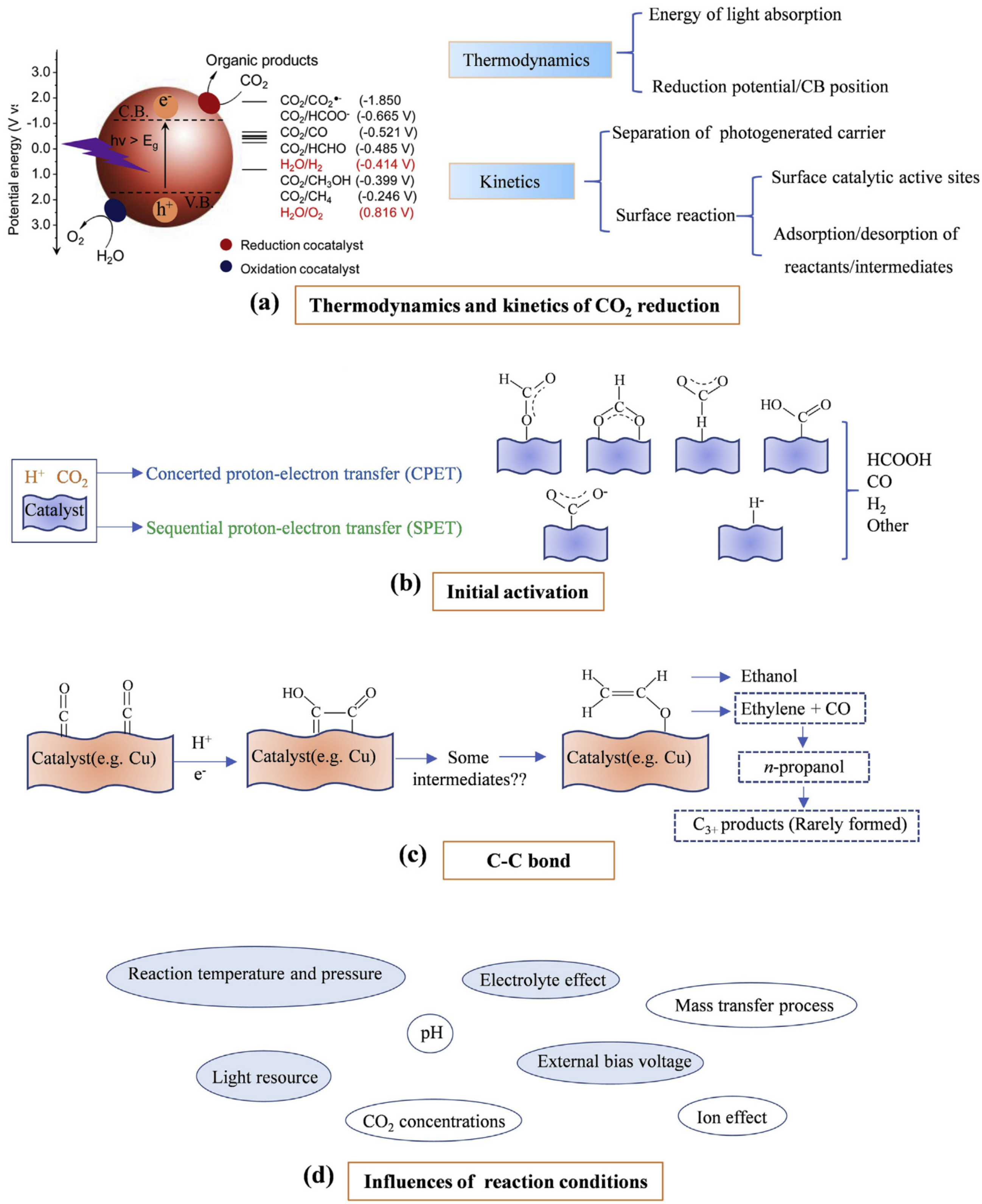

Fig. 4. Influence factors of photoelectrocatalytic CO_2 reduction. (a), Thermodynamics and kinetics on photoelectrode [20]. Reproduced with permission: Copyright 2017, American Chemical Society. (b), Initial activation of CO_2. (b) The C–C bond formation to generate C_2H_4 and C_{3+} products. (d) The external conditions, including light source, PH, Ion effect and so on.

the intermediates generated via CO_2 activation in SPET are generally charged (or strongly polarizable), which is susceptible to pH and cation effects [13]. Therefore, the activation of CO_2 is important to affect the reaction efficiency and product selectivity.

4.2.2. C–C bond formation

During the CO_2 reduction reaction (CO2RR), one or more C–C bonds were usually formed on copper-based electrodes during CO_2 reduction, which can realize the selectivity improvement of C_2 products by tuned the structure of copper [101,102]. In addition, NiGa, PdAu, and NiP catalysts were also reported to generate C_2 or other more carbon products while the efficiency is different from that of copper [103–106]. The most typical multi-carbon products in liquid phase reduction of CO_2 are ethylene and ethanol, which have high energy density and economic value [107]. The production of ethylene include two pathways: one is the high-overpotential pathway mainly occurred on Cu (111) with the generation of intermediate such as methane, while another is the low-overpotential pathway mainly occurred on Cu (100) without producing C_1 products [108]. The pH dependence of these two pathways is also different, the former pathway is PH dependent while the latter pathway is not, which makes CO_2 and CO have (local) high pH sensitivity on copper-based catalyst. Several experimental and theoretical studies have indicated the key intermediate is a CO dimer in this pathway to form C_2 product [109–113]. The DFT calculation shows that CO dimerization is not easy to occur at a more negative potential, and the coupling reaction of *CO and *CHO has a lower activation energy [113]. Combined with the results of experiments and DFT calculations, the rate of C–C coupling is determined by the proton-electron transfer involved in the step, and explain its PH sensitivity [111]. In alkaline LiOH electrolyte, the presence of hydrogen CO dimer intermediate (OCCOH) can be observed in Fourier infrared spectroscopy, which further certified the formation of C–C coupling is sensitive for structure and PH [114]. In addition to ethylene, other C_2 products including acetaldehyde and ethanol can also be observed in CO_2 reduction. The hydrogenation of intermediates promotes acetaldehyde and ethanol formation, and then the hydrogenolysis of intermediates induces the formation of ethylene [111]. The formation of advanced (C_{3+}) hydrocarbons with the FE of 20% has also been observed on appropriated copper [115]. Additionally, the propanol and propanal are main C_3 products observed, also including a small amount of hydroxyacetone, allyl alcohol and acetone. The basic formed pathways of these C_3 products have not been studied clearly yet. There is literature has been reported that C–C coupling between CO and C_2H_4 precursors would form *n*-propanol [116]. Fig. 4c shown the formation of C–C bond related to C_2H_4 and C_{3+} products on the surface of catalyst e format. Based on the above discussion, the selectivity of products can be optimized by tuning photoelectrocatalyst structure to form C–C bonds during CO_2 reduction.

4.3. Reaction conditions

4.3.1. Light source

For the system of photoelectrocatalytic CO_2 reduction, the energy of light plays an important role for semiconductor to generate excited electrons in the system [64]. First, different reaction systems (mainly gas reaction system and liquid reaction system) have different requirements for light sources. Research shows that the ultraviolet ray drastic decay from gas phase into liquid phase [117,118]. Therefore, the UV light source should be fully considered the light source intensity, distance of light source to electrode and other factors in the liquid-phase reaction system. Additionally, different photoelectrodes need different excitation energies due to the differences of band gaps. When selecting a light source, the emitted light must contain the wavelength portion of the excitable semiconductor. At present, the most ideal light source is the sun. Its spectrum consists of about visible light (wavelength $\approx$ 400–760 nm), infrared light (wavelength $>$ 760 nm) and ultraviolet light (wavelength $<$ 400 nm). Among them, UV can stimulate most semiconductor catalysts to produce photogenerated electrons. The synthetic light source mainly includes metal halide lamp, mercury lamp, ultraviolet lamp, xenon lamp and LED [119–121]. The wavelength of the synthetic light source can be adjusted according to the different experimental parameters, but the main drawback is the need for additional power to drive, thus increasing energy consumption. So far, most of the basic research in laboratory is to use artificial light source for conventional research, and finally to carry out experiments with the sun as the light source for industrial application. In the future, the solar light source is the ultimate goal for photoelectrocatalytic CO_2 reduction from laboratory to large-scale use. Therefore, the reaction system integrated solar cell might be a good development direction.

4.3.2. Reaction temperature and pressure

The influence of temperature on the efficiency of photoelectrocatalytic CO_2 reduction mainly focused on these aspects including dissolution, diffusion and/or migration of CO_2 molecules. In the liquid phase reaction system, there are two following situations. On the one hand, the HCO_3^- or CO_3^{2-} ions would be generated by CO_2 dissolved in water, and movement speed of them also accelerates with the increase of temperature, which can promote the reaction [61,122]. And there is molecular state of CO_2 in the liquid phase system saturated with CO_2, which can directly obtain the photogenerated electrons and be converted when the temperature is appropriate. But on the other hand, the temperature causes the gas solubility to decrease and the high temperature causes the system energy consumption to increase greatly [61]. In photoelectrocatalytic CO_2 reduction, the main purpose is to achieve energy conservation and environmental protection, so the reaction temperature should be carefully considered. Additionally, the pressure of CO_2 also affects the solubility. The CO_2 concentration in solution can be increased under high-pressure environment, promoting higher photoelectrocatalytic current density and CO_2 reduction rate. In addition, some reports showed that the high CO_2 pressure could also enhance the CO_2 reduction rather than proton reduction, improving the stability of photocathode and product selectivity [61,123,124].

4.3.3. Electrolyte effect

The electrolyte effect (pH, ion effect, the CO_2 concentration and mass transfer process, etc.) will affect the reduction efficiency and product selectivity [125]. The pH, electrolyte composition and buffer capacity can influence on CO_2/HCO_3^-, H_2CO_3/HCO_3^- and HCO_3^-/CO_3^{2-} equilibria in water, which makes carbonaceous species have different concentrations in solution [126–128]. Compared with other electrolytes, bicarbonate electrolyte can enhance CO_2 reduction activity because of the formation of bicarbonate-CO_2 complex, which is as the main carbon source during the CO_2 reduction period, inducing CO_2 concentration to increase in near the electrode. The existence of bicarbonate was proved by isotope labeled infrared spectroscopy [129]. During CO_2 reduction, the alkaline pH close to the electrode was higher than that of base solution because of the formation of hydroxide. This locally alkaline pH is the result of mass transfer and changes in local pH are proportional to current density, depending on factors such as the nature of the electrolyte and buffering capacity, as well as the shape of the electrode [130–132].

The properties of cations and anions in electrolytes importantly affect the reduction efficiency and product selectivity in CO_2 reduction. Generally, larger cations in electrolytes can bring about a higher C_2/C_1 ratio and a higher CO_2 reduction rates on copper electrodes [13,133]. The cation hydrolysis effect can increase local concentration of dissolved CO_2 because the buffering was enhanced near the electrode for larger cations [133]. Researches show that the onset potential for ethylene depends on the nature of cation while that for methane was unrelated to cation size [134]. In terms of halide adsorption on catalyst surface, anion effects are generally explained as changing the electronic structure, and subsequently enhancing reduction efficiency and product selectivity. And the halide size and concentration also affect the efficiency of CO_2 reduction [135]. The relationship between reaction conditions and the

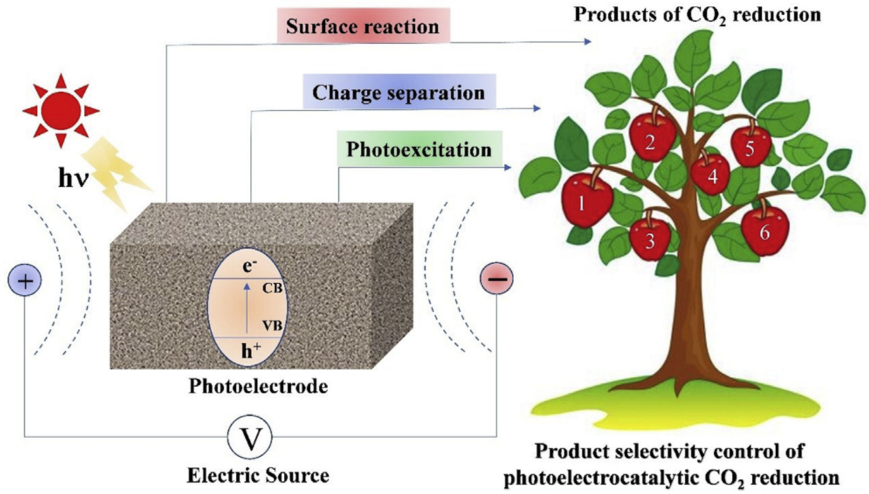

Fig. 5. Main optimizing process for enhancing product selectivity of photoelectrocatalytic CO_2 reduction on photoelectrode.

individual effects mentioned above is very important, but which is still poorly understood.

4.3.4. External bias voltage

In the process of photoelectrocatalytic CO_2 reduction, the external bias voltage can effectively separate photogenerated electron-hole pairs, thus improving the photoelectrocatalytic efficiency on photoelectrode. Hasan et al. [136] studied the CO_2 reduction performance during the voltage range was −1.5–0.0 V, finding that the products were mainly formic acid (HCOOH) and methanol (CH_3OH) under −0.61 V bias. Generally speaking, there is an optimization condition between the external bias voltage and the photoelectrocatalytic CO_2 reduction conversion rate. Under the optimal bias voltage condition, separation efficiency of photogenerated electron-hole pairs reaches the maximum. If the external bias voltage continues to increase, the photoelectrocatalytic CO_2 reduction efficiency will no longer increase. Additionally, excessive bias voltage will not only increase the reduction products and reduce the selectivity of the products, but also increase the energy loss of the whole photoelectrocatalytic CO_2 reduction system. Therefore, the effect of external bias voltage on the reduction performance should be investigated in the actual photoelectrocatalytic CO_2 reduction system so as to find the best bias voltage.

5. Enhancement strategy of photoelectrocatalytic performance

Recently, much progress has been developed in photoelectrocatalytic CO_2 reduction. Castro et al. [59] reviewed the main materials of photoelectrodes, photocatalytic reactors of different configurations and their characteristics. Which provides a deep understanding on the photoelectrocatalytic CO_2 reduction from the aspects including photoelectrode structures and photoelectrocatalytic reactor. Simultaneously, the application of photoactive materials and key variables of configuration in reaction performance are also discussed. Gong et al. [60] reviewed the research progress of cocatalyst modified semiconductor based photoelectrode from the perspective of material modification, discussed the role of cocatalyst in reaction, and summarized the relationship between the performance of the photoelectrode and its structure. Xiong et al. [61] started from the fine structure of the photocathode, summarized strategies including improving the light utilization rate, providing catalytic active sites and controlling reaction paths, and summarized various novel photoelectrocatalytic CO_2 reduction reaction devices.

Crucially, the important aim in photoelectrocatalytic CO_2 reduction is to obtain high yield of target product. However, the undesired byproducts were generally produced by consume valuable photogenerated electrons on the surface, which makes the output of target products obviously lower. The poor product selectivity usually leads to the mixing of multiple products, which leads to another challenge that is to separate valuable target products from mixed products. Therefore, enhancing the product selectivity in the reaction process of photoelectrocatalytic CO_2 reduction is one of the keys to realize its application [87,90,91]. The main process of photoelectrocatalytic CO_2 reduction is that the semiconductor photoelectrode generates electrons by photoexcitation, and electrons transfer to electrode surface under the guidance of external voltage to carry out the catalytic reaction of CO_2 reduction. The structure and reaction characteristics on photoelectrode are the key factors affecting the efficiency and selectivity of photoelectrocatalytic CO_2 reduction. Therefore, product selectivity of photoelectrocatalytic CO_2 reduction can be adjusted by optimizing the multiple process in terms of photoexcitation, charge separation efficiency and surface reaction on photoelectrode, as shown in Fig. 5. The main strategies for enhancing the reaction efficiency and product selectivity of photoelectrocatalytic CO_2 reduction on photoelectrode include photoexcitation (e.g., doping element, introducing surface plasmon and quantum dots), charge separation efficiency (e.g., loading co-catalysts, constructing heterojunction and defect structure), surface reaction (e.g., adsorption and activation of reactants, adsorption/desorption of intermediates), and their synergistic effects. In the following parts, we will discuss the methods, structural properties and mechanisms involved in above process.

5.1. Photoexcitation

The energy of light absorption determines whether the semiconductor can be excited and how many electron-hole pairs can be generated, which affects reaction rate and product selectivity of CO_2 reduction from thermodynamic [87,137]. In semiconductor photoelectrode, the band gap can generally determine the excitation energy needed, thus wavelength range of the incident light to be used. Additionally, the CB position (i.e., reduction potential) of photoelectrode is greatly related to the reduction abilities of photogenerated electrons. Adjusting the band structure of photoelectrode can optimize reduction potentials of electrons, which can effectively regulate the product selectivity from thermodynamics. Doping is an effective method to adjust band structure of photoelectrode, which can control the thermodynamic CO_2 reaction and thus greatly affect the product selectivity. Gu et al. [138] reported a *p*-type Mg-doped $CuFeO_2$ electrode, which realized photoelectrochemically reduce CO_2 to formate at an underpotential (400

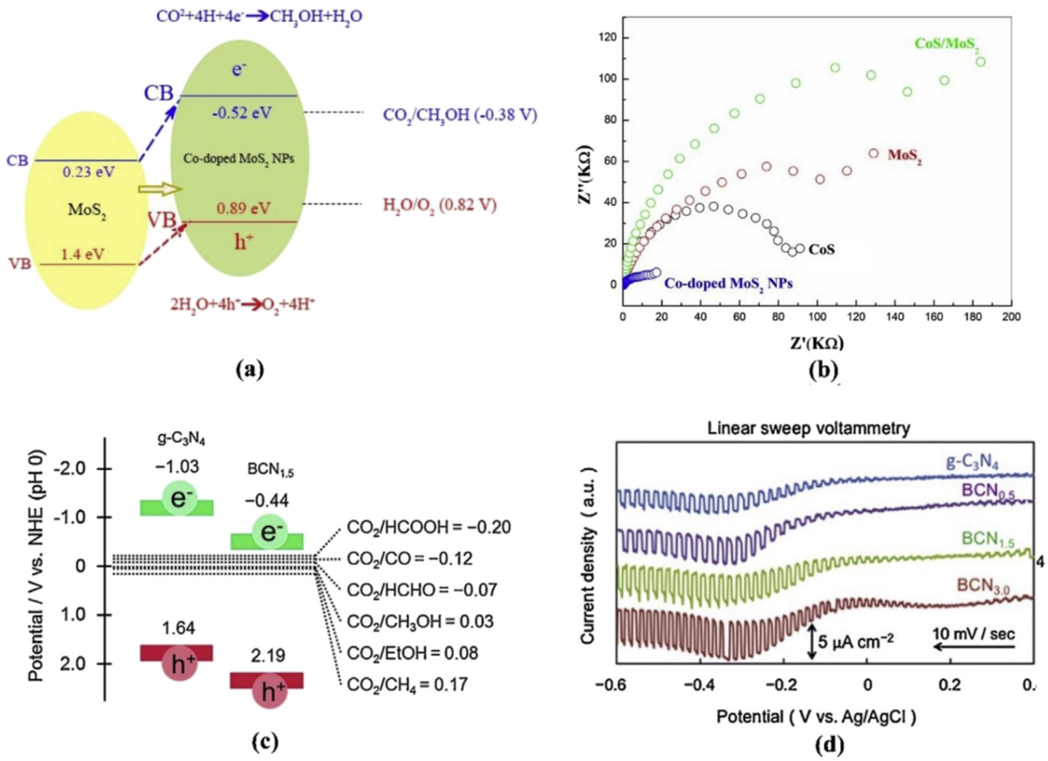

Fig. 6. (a) Reduction mechanism of CO_2 on the Co-doped MoS_2 NPs and (b) Electrochemical impedance spectroscopy of samples [139], Reproduced with permission: Copyright 2015, Elsevier. (c) The band potential diagram of B-doped g-C_3N_4 ($BCN_{1.5}$) and (d) photocurrent of CO_2 reduction on BCN_x [140]. Reproduced with permission: Copyright 2016, Elsevier.

mV). The introduction of Mg enhanced the visible light absorption and current density. When the applied electrode potential is −0.4 V vs SCE, irradiating with wavelength of ~800 nm can produce photocurrent, and a value of 14% for photon-to-current efficiency can be obtained at 340 nm. Peng et al. [139] prepared Co-doped MoS_2 NPs and used for photoelectrocatalytic CO_2 reduction. The Co element upshifted CB position, which makes the band gap of MoS_2 is narrowed and resistance is also reduced. Therefore, the photoelectrocatalytic performance of reducing CO_2 to methanol is excellent (Fig. 6a and b). Sagara et al. [140] prepared a *p*-type boron-doped g-C_3N_4 (BCN_x) electrode for photoelectrochemical reduction of CO_2 under visible light irradiation. The BCN_x not only obviously changed the energy band structure (Fig. 6c), but also showed a remarkable *p*-type conductivity. Additionally, the photocurrent was greatly enhanced in $BCN_{3.0}$ (Fig. 6d), and the main product is C_2H_5OH. At present, the self-doping of photoelectrode was rarely reported for photoelectrocatalytic CO_2 reduction. But we believe it can be developed for optimizing photoelectrodes to improve the reduction efficiency of CO_2 in near future.

In addition, if plasmonic photocatalyst is used as photoelectrode, which shows different light absorption and excitation modes compared with traditional semiconductor-based photoelectrode, which can obtain strong light absorption via localized surface plasmon resonances. The adsorbed reactants can be activated by energetic (hot) electrons, promoting the reaction of CO_2 reduction. The energy and density of the photons greatly affect the distribution of photoexcited hot electrons, leading to different reaction rates and pathways [141–145]. DuChene et al. [141] fabricated gold/*p*-type gallium nitride (Au/*p*-GaN) Schottky junctions and studied the capture and conversion plasmon-induced hot-hole in photoelectrochemical reactions. The Au/*p*-GaN can keep a sustained photovoltage by plasmon excitation (Fig. 7a), which makes the selectivity of CO generation greatly improve in aqueous electrolytes by plasmon-driven photoelectrochemical CO_2 reduction (Fig. 7a). Kim et al. [142] demonstrated the enhanced photoelectrochemical performance of CO_2 reduction via surface plasmon on silver nanostructured electrodes. Under light irradiation, the photogenerated plasmonic hot electrons of nanostructured silver electrodes would transfer to the lowest unoccupied molecular orbital (MO) acceptor energy levels of adsorbed CO_2 or their reductive intermediates, which can enhance the yield, efficiency and selectivity of photoelectrochemical processes. In addition to Au, Ag and other precious metals, Cu also has plasma effect. Shen et al. [144] decorated metallic Cu nanoparticles in Co_3O_4 nanotube arrays (Fig. 7b), which showed a high selectivity of formate in photoelectrocatalytic CO_2 reduction. Therefore, it is feasible to control the product selectivity by adjusting the photoexcitation of plasmonic photoelectrode.

Moreover, the introduction of dye molecules and quantum dots (QDs) into the photoelectrode can also effectively enhance the light absorption. Xu et al. [146] reported that the introduction of Eosin Y disodium salt can improve light absorption. Simultaneously, the introduced Pd nanoparticles and amine ligands can capture protons and CO_2, respectively. The major liquid product was methanol, and the highest selectivity reached approximately 100%. The schematic diagram of catalyst action is shown in Fig. 8a. Isaacs et al. [147] reported that it was possible to modify ITO electrodes with assemblies (polycations/QDs), with polycations PDDA and PMAEMA. Polycations can limit the effects of light on the QDs photoelectrocatalytic properties because different monomer structures of Polycations will generate different arrangements in the assemblies. The modified electrodes with $(PMAEMA/QDs)_6$ assemblies exhibited better selectivity of HCOH during photoelectrocatalytic CO_2 reduction (Fig. 8b).

5.2. *Charge separation efficiency*

The separation efficiency of photogenerated electron-hole pairs greatly determines the density of photogenerated electrons on photoelectrode surface [148–151]. The electron density would strongly affect the multi-step reactions of CO_2 reduction, leading to different conversion

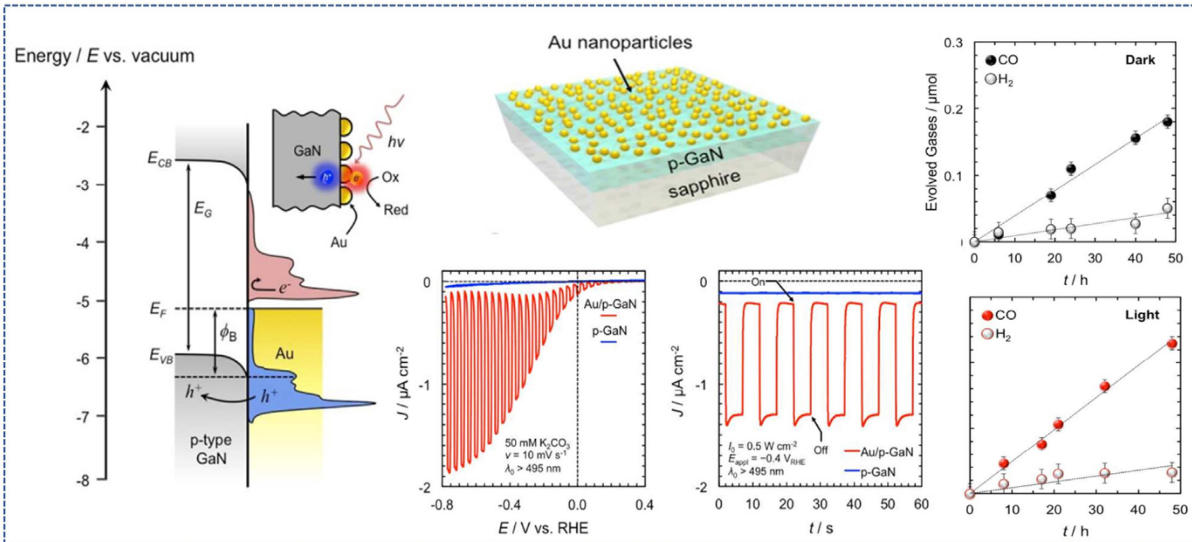

(a) Au plasma

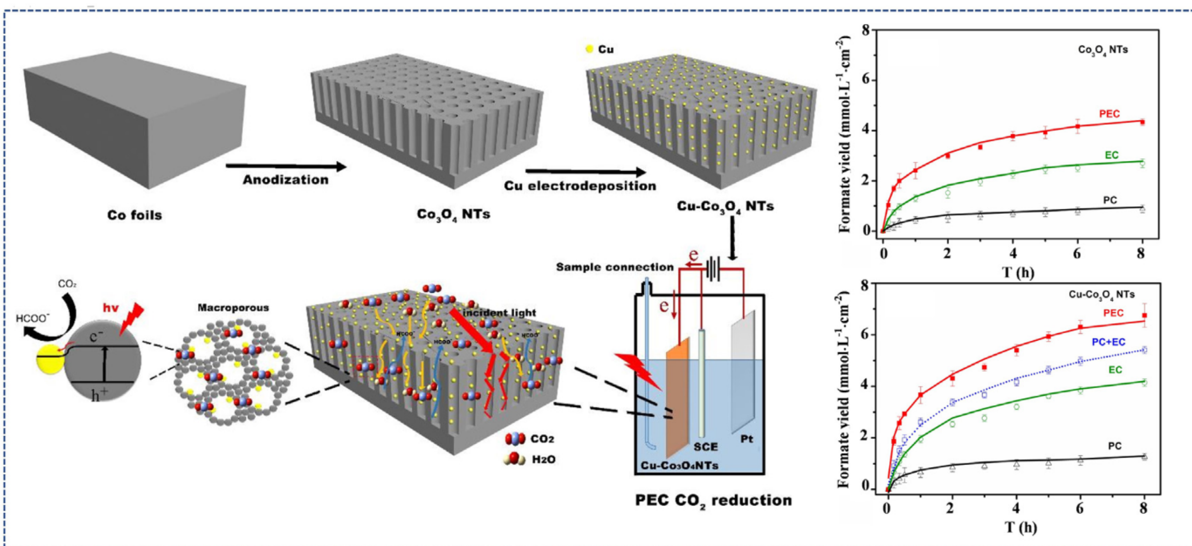

(b) Cu plasma

Fig. 7. The plasmonic photoelectrodes improved activity and selectivity of photoelectrocatalytic CO_2 reduction. (a) Au/*p*-GaN photocathodes with plasma effect [141], Reproduced with permission: Copyright 2018, American Chemical Society. (b) Cu–Co_3O_4 NTs photocathode with surface plasmon [144]. Reproduced with permission: Copyright 2015, American Chemical Society.

pathways to obtain different products. Therefore, enhancing the electron-hole separation efficiency in photoelectrode should be a critical strategy to regulate product selectivity [152–154]. The external voltage can promote the separation and transfer of photogenerated carriers, and obtain higher density of photogenerated electrons on photoelectrodes for CO_2 reduction, which is a major feature and advantage of photoelectrocatalytic CO_2 reduction. The higher surface electron density can obviously change the product selectivity [136,147]. Besides, utilizing surface modification or interface control to optimizing photoelectrodes, such as loading metal co-catalysts, constructing heterojunction and defect engineering, can be an effective way to enhance the efficiency of photogenerated electron-hole separation and obtain high surface electron density.

5.2.1. Loading metal co-catalysts

A large overpotential generally needs to overcome caused by kinetic sluggishness of multi-electron reactions, which make the efficiency of CO_2 reduction be limited. Loading co-catalysts on semiconductor is believed an effective method to enhance efficiency of photocatalytic CO_2 reduction [70,155–159]. The overpotential and energy barrier can be reduced via the effects of co-catalysts, promoting CO_2 activation. Additionally, the co-catalysts can also promote the transfer of photogenerated charge carriers to reactants, accelerating surface reaction from kinetics. Moreover, selecting appropriate co-catalysts can restrain side or back reaction to design reduction pathway, improving product selectivity. Therefore, co-catalysts can be used to improve the reaction efficiency and product selectivity of photoelectrocatalytic CO_2 reduction. The mechanisms and fundamentals of loading co-catalysts on semiconductor photoelectrodes will be discussed in this section.

The metal co-catalysts generally have two positive roles: 1) capturing photogenerated electrons to promote carrier separation; and 2) acting as catalytic active sites to reduce overpotential and carry out the reaction [156,160,161]. The Schottky junction at the interface would be formed by directly loading metal nanoparticles on semiconductor, which will

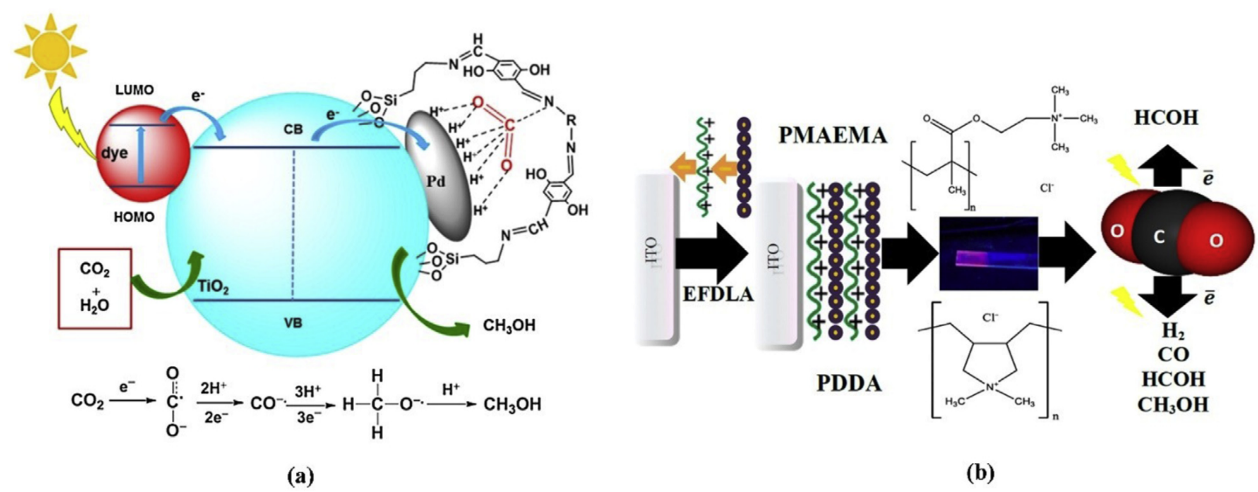

Fig. 8. (a)Schematic reduction mechanism of CO_2 on multi-functionalized TiO_2 photocathodes [146], Reproduced with permission: Copyright 2017, Elsevier. (b) Schematic diagram of electrode assembly and photoelectrocatalytic CO_2 reduction of quantum dot-modified electrodes [147]. Reproduced with permission: Copyright 2015, American Chemical Society.

affect the charge transfer. If the work function of *p*-type semiconductor is larger than that of metal, the electrons on metal surface would transfer to semiconductor after contact. But in photoelectrocatalytic system, which is different. For *p*-type semiconductor photocathode, the separated photoinduced holes would transfer to the counter electrode to trigger oxidation reaction through the external bias under light irradiation. And the electrons would accumulate on metal of photocathode surface to promote CO_2 reduction. Although many metals as co-catalysts exhibited excellent performance, not all metals are suitable candidates for photoelectrocatalytic CO_2 reduction. And the biggest concern is that some metal co-catalysts would lead to serious competitive reactions such as H_2 evolution [93,122]. Fig. 9 shows that the typically metal electrodes are categorized by their primary products in solution: formic acid, carbon monoxide, or hydrogen. Copper is widely used in electrocatalytic CO_2 reduction due to the ability to produce a variety of hydrocarbons [122]. Therefore, an excellent metal co-catalyst should simultaneously realize the improvement of Faradaic efficiency and suppression of competitive reactions in photoelectrocatalytic CO_2 reduction.

In recent years, the effect of loading metal co-catalysts on photoelectrodes was investigated for photoelectrocatalytic CO_2 reduction [162–164]. For example, *p*-Si photocathode was modified by Cu, Ag and Au nanoparticles for photoelectrocatalytic CO_2 reduction. Fig. 10a and b showed the mechanism diagram of photoelectrocatalytic CO_2 reduction. The main products were CO and HCOOH for Ag and Au, while the Cu cocatalyst could induce CH_4 and C_2H_4 to produce [163]. Similarly, Pb, Ag, Au, Pd, Cu and Ni as co-catalysts on *p*-InP photocathode were also studied in photoelectrocatalytic CO_2 reduction. Both CO and HCOOH can be produced by Pb, Ag, Au and Cu co-catalysts while the only product was CO via Pd modification according to the experiments. The selectivity of products was related to the different enthalpy and Gibbs energy of dissociative adsorption of CO(g) on metal surface [162]. Jang et al. [165] designed a new Au-coupled ZnTe/ZnO-nanowire photocathode for selective CO_2 reduction to CO. In general, the H_2 evolution was verified to be the dominant competitive reaction on ZnTe/ZnO, which is attributed to its negative CB position. When Au nanoparticles were as co-catalyst on ZnTe/ZnO surface, the activity and selectivity were enhanced (Fig. 10c–e). Additionally, Au, Ag, Cu, etc. metals have plasmon effect and can be loaded on the photoelectrode to achieve enhancement of light excitation and charge separation to control the product selectivity, which have been discussed in above section of photoexcitation [141,142,144].

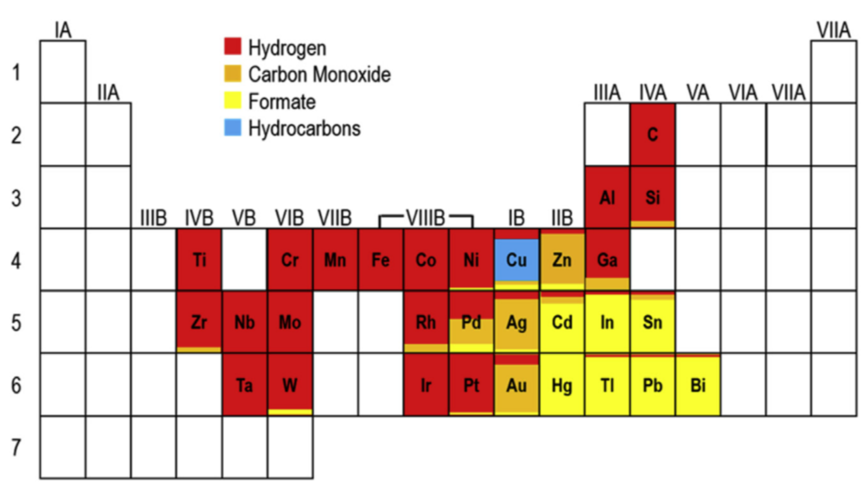

Fig. 9. Periodic table depicting the primary reduction products in CO_2-saturated aqueous electrolytes on metal and carbon electrodes [122]. Reproduced with permission: Copyright 2015, American Chemical Society.

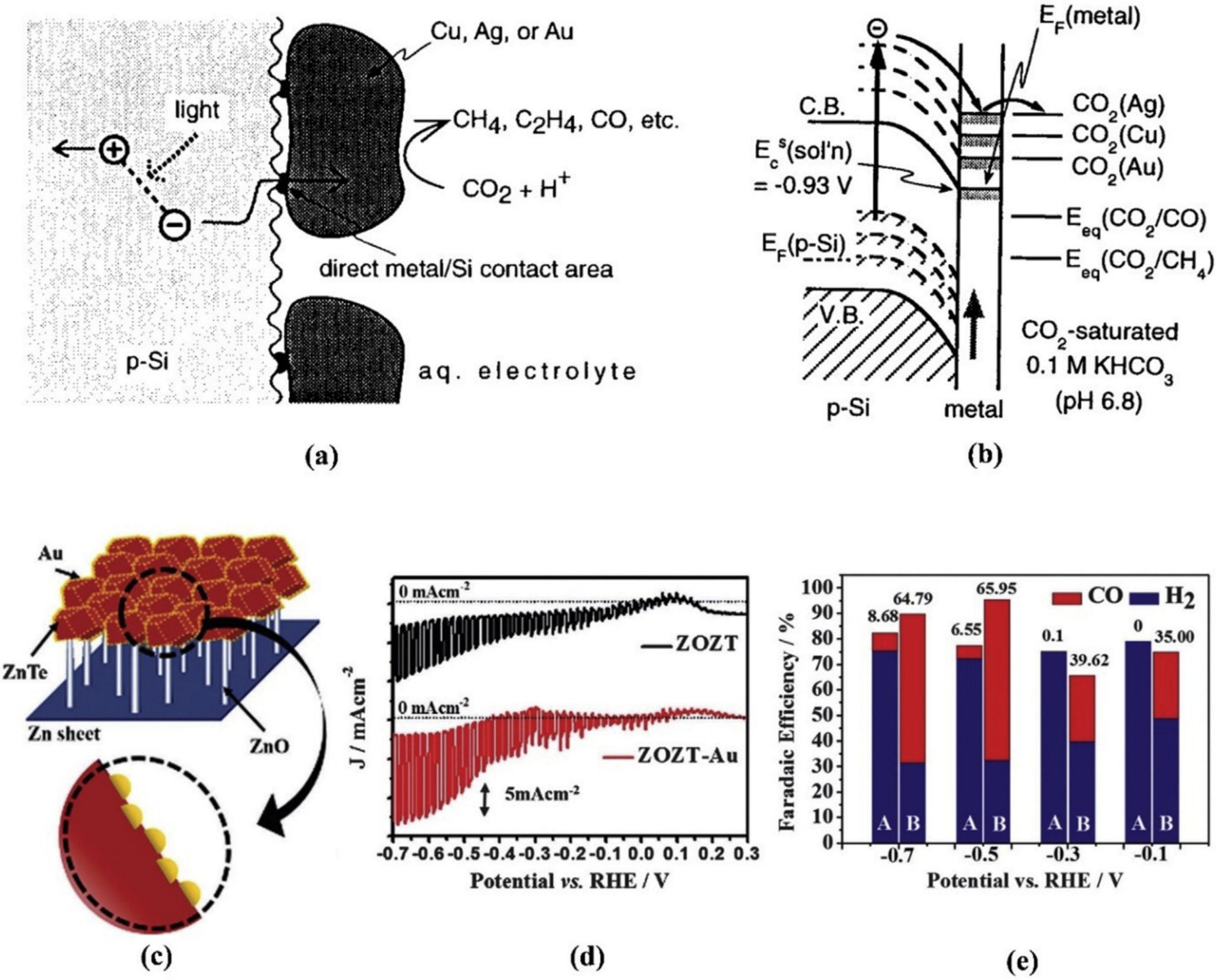

Fig. 10. (a) Schematic of metal particles modifying *p*-Si electrodes and (b) Energy band diagrams of particulate-metal/*p*-Si [163], Reproduced with permission: Copyright 1998, American Chemical Society. (c) Schematic of the Au coupled ZOZT composite, (d) Photocurrent response and (e) FEs of CO and H_2 from the photoelectrocatalytic CO_2 reduction with ZnTe/ZnO (A) and Au-coupled ZnTe/ZnO (B) photocathodes [165]. Reproduced with permission: Copyright 2015, Royal Society of Chemistry.

Therefore, selecting suitable metals as co-catalysts loaded on photoelectrode is feasible to improve efficiency and selectivity of photoelectrocatalytic CO_2 reduction.

5.2.2. Constructing heterojunction

The construction of heterojunction is an effective strategy to improve the separation efficiency of photogenerated electron-hole pairs in photocatalytic process. The heterojunctions include various types, such as

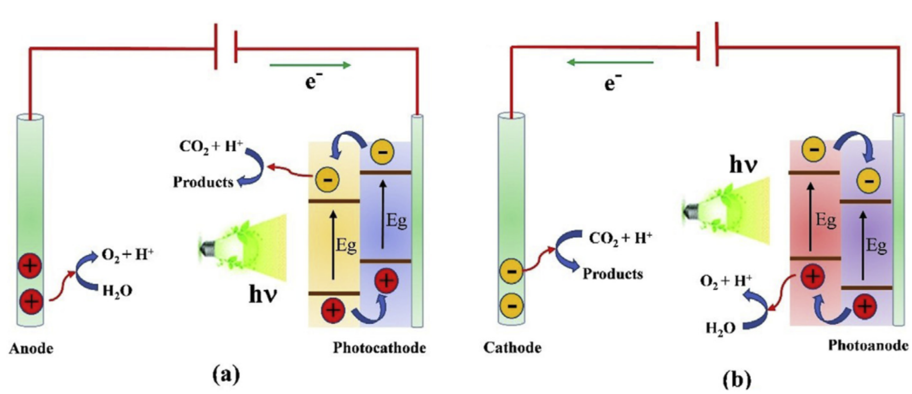

Fig. 11. Schematic diagrams for photoelectrode: (a) photocathode, (b) photoanode.

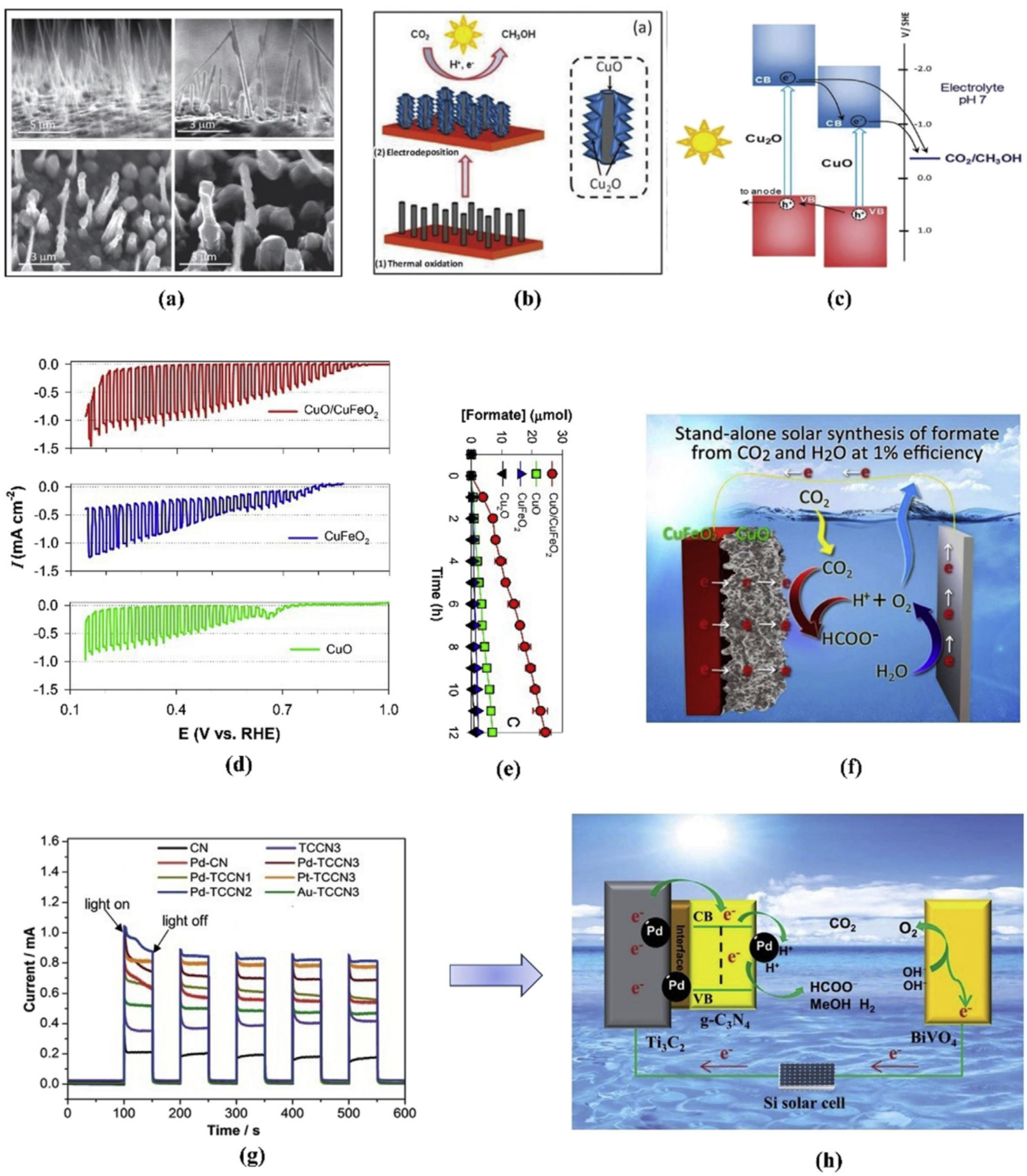

Fig. 12. (a) Morphology of a CuO–Cu_2O nanorod, (b) Schematic of synthesizing CuO–Cu_2O hybrid nanorod arrays, (c) Energy band diagram of CuO–Cu_2O and mechanism for solar CO_2 [170], Reproduced with permission: Copyright 2013, Royal Society of Chemistry. (d) Linear sweep voltammograms for $CuFeO_2$/CuO, (e) Formate productions, (f) Mechanism of photoelectrocatalytic CO_2 reduction on $CuFeO_2$/CuO photocathode [173], Reproduced with permission: Copyright 2015, Royal Society of Chemistry. (g) Transient photocurrent responses, (h) Proposed mechanism for PEC reduction of CO_2 into chemical fuels [174]. Reproduced with permission: Copyright 2018, Royal Society of Chemistry.

conventional type-II heterojunction, metal–semiconductor (m–s) junction, p–n junction, direct Z-scheme heterojunction, and surface heterojunction, which are feasible to separate photogenerated electrons and holes [166–168]. By constructing heterojunction, the recombination of photogenerated carriers can be greatly reduced during migration process, promoting more electrons to reach the surface of photocatalyst and thus obtaining higher surface electron density. The multi electron reactions would be more easily to occur under higher surface electron density, which can facilize the generation of higher reduced state products. Therefore, product selectivity is related with the migration process of carriers through heterojunction.

Although constructing heterostructure to effectively improve charge separation efficiency is widely studied in photocatalysis, it is developing and need to strengthen the research in photoelectrocatalysis [169]. In terms of photoelectrocatalytic system, the type-II heterostructure was most widely studied and Fig. 11 shown the heterostructure of photoelectrode. The photogenerated electrons migrate from the semiconductor with a higher CB to that with a lower CB Under light irradiation, while holes would be accumulated at the semiconductor with higher VB. Driven by external voltage, photogenerated electrons are accumulated at the CB of photocathode to carry out CO_2 reduction, while holes are migrated to the counter electrode to participate in H_2O oxidation. For photoanode, the photogenerated electrons are moved to the counter electrode and conduct CO_2 reduction while holes are left to carry out H_2O oxidation. Through designing heterostructure and adjusting external electric field, the charge will be highly separated and thus enhancing the efficiency of photoelectrocatalytic CO_2 reduction.

Ghadimkhani et al. [170] prepared CuO–Cu_2O nanorod arrays as *p*-type semiconductor photocathode to carry out photoelectrocatalytic CO_2 reduction. Fig. 12a and b showed the prepared approach and microstructure of CuO–Cu_2O nanorod arrays. Fig. 12c exhibited the mechanism of charge separation and migration at the interface by strong

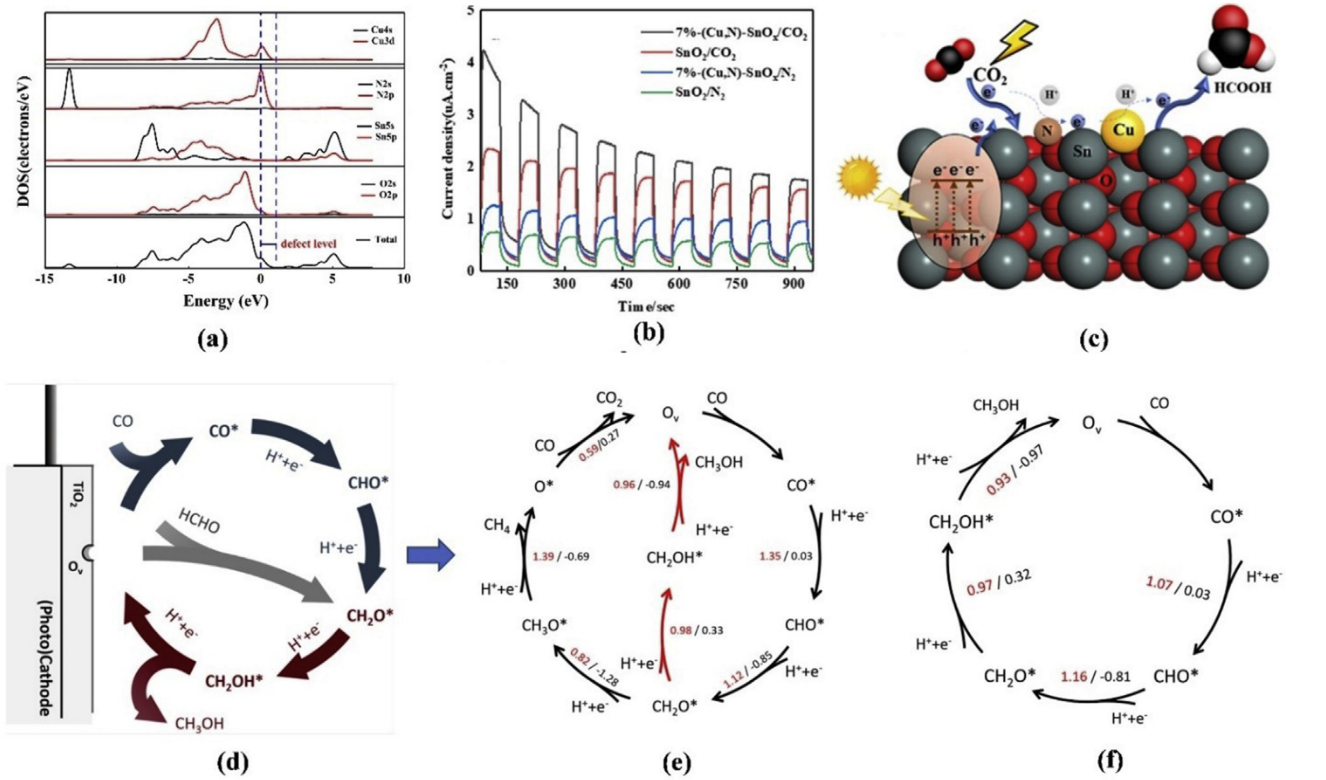

Fig. 13. (a) Density of states for co-doping SnO_2, (b) Transient photocurrent responses, (c) Mechanisms of photoelectrocatalytic CO_2 reduction on the (Cu, N)-SnO_x [185], Reproduced with permission: Copyright 2020, Elsevier. (d) Schematic diagram of the CO_2 (CO) reduction catalytic cycle on the defective anatase surface: (e) at the S/C interface, (f) at the E/C interface [180]. Reproduced with permission: Copyright 2020, American Chemical Society.

electric field built-in electric field. At an underpotential, CuO–Cu_2O photocathode exhibited an excellent photoelectrocatalytic CO_2 reduction to methanol. Additionally, Takanabe et al. [171] also reported a Cu_2O/CuO heterojunction photocathode on Cu foil, which made CO_2 reduce to CO with 60% selectivity under constant current conditions (-1.67 mA·cm^{-2}) at -0.6 V *versus* RHE. Moreover, Won et al. [172] pointed out that Cu_2O/Cu would be produced on the surface by reduced from CuO (CuO/Cu_2O photocathodes), which would destroy the electron–hole pathways. Other Cu-based heterojunction photoelectrodes also showed excellent performance for CO_2 reduction. Kang et al. [173] prepared a $CuFeO_2$/CuO catalyst for photoelectrochemical CO_2 reduction. The $CuFeO_2$/CuO photocathode exhibited an enhanced photocurrent (Fig. 12d) and improved photoelectrocatalytic performance of CO_2 reduction (Fig. 12e). The selectivity of formate was over 90% under simulated solar light. Fig. 12f showed the mechanism of photoelectrocatalytic CO_2 reduction on $CuFeO_2$/CuO photocathode. Additionally, Xu et al. [174] fabricated Ti_3C_2/g-C_3N_4 (TCCN) heterojunctions for photoelectrocatalytic CO_2 reduction. The heterojunction not only enhanced light absorption but also promoted the charge separation to increase the photocurrent (Fig. 12g). On the basis of the heterojunction, the modification by nanometal particles would further accelerate charge transfer to improve surface electron density. And mechanism for charge separation and CO_2 reduction is proposed in Fig. 12h.

5.2.3. Defect engineering

For photocatalysis and electrocatalysis, defect engineering has been developed to increase the carrier separation efficiency, promote adsorption activation of reactants, enhance reaction efficiency and product selectivity [47,175–181]. Higher electron density can be obtained at defect positions, and importantly affect the product selectivity of multi-electron reaction involved in CO_2 reduction. However, some other studies present that defects could also adversely perform as the electron–hole recombination centers, leading to decrease photocatalytic activities [182,183]. Notably, these contradictory effects of defects might due to the complex defect structures closely related to photocatalytic activity and selectivity. However, there is still a lack of advanced *in-situ* characterization techniques to characterize the complex relationship between structure and properties. Zhang et al. [184] pointed out that the defects cannot only serve as active sites for molecular chemisorption, but also spatially supply channels for energy and electron transfer. They emphatically outline how the parameters of defects (e.g., concentration, location, geometric and electronic structures) can serve as the knobs for maneuvering molecular adsorption and activation as well as altering subsequent reaction pathway. Moreover, Wang et al. [177] summarized the design methods of surface defects and functional interface from atomic-level in electrocatalysts to promote efficiency and selectivity. Xue et al. [178] summarized the construction of the diverse defect types for carbon materials in electrocatalytic CO_2 reduction, and revealed the relationship between structure and activity of CO_2 reduction.

According to above analysis, we believe that adjusting the defect structure of the catalyst should be applicable for photoelectrocatalytic CO_2 reduction. But the current photoelectrocatalytic research is in a relatively initial stage, and the understanding of defect promoting the photoelectrocatalytic performance remains to be developed. Yang et al. [185] reported a Cu and N co-doped SnO_2-based catalyst with defect for photoelectrocatalytic CO_2 reduction. The DFT revealed that the defect levels can narrow band gap for accelerating charge transfer, thus improving the photoelectrocatalytic performances in CO_2 reduction to formate (Fig. 13a–c). Additionally, Yuan et al. [180] uses DFT to study photoelectrocatalytic CO_2 reduction on the defective TiO_2 surface (Fig. 13d), at both solvent/catalyst and electrolyte/catalyst interfaces. Their study revealed an essential role of oxygen vacancy in the reduction process. The defect can promote the adsorption and activation by charge transfer between defective site and chemical adsorbed molecules on the

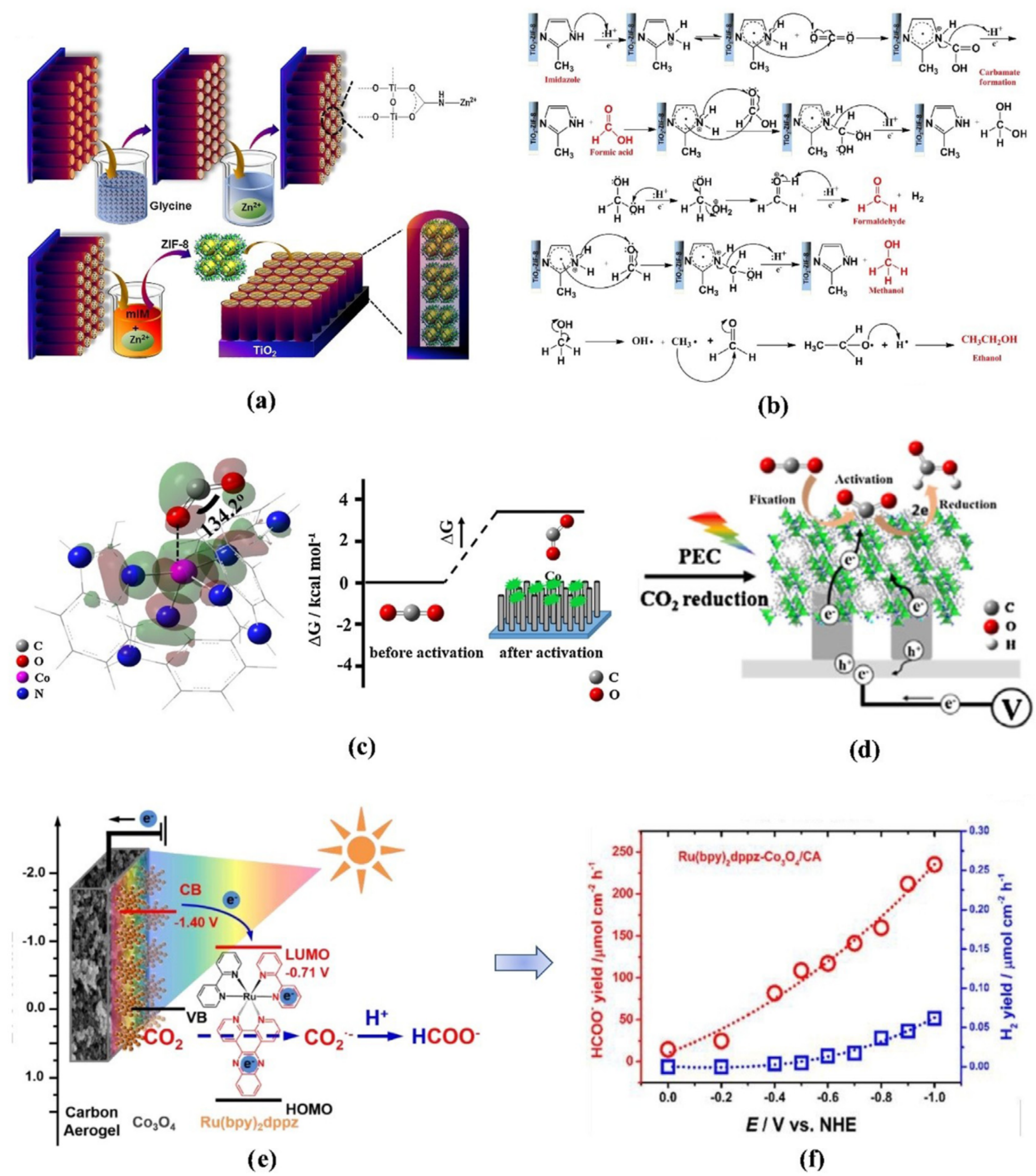

Fig. 14. (a) ZIF-8 formation on Ti/TiO_2NT, (b) Formation mechanism of alcohol on Ti/TiO_2NT-ZIF-8 electrodes [196], Reproduced with permission: Copyright 2018, Elsevier. (c) The adsorption mode of CO_2 and Gibbs energy by DFT calculation (d) Mechanism of PEC CO_2 reduction on ZIF9-Co_3O_4 NWs [197], Reproduced with permission: Copyright 2017, Elsevier. (e) Conversion pathways of CO_2 on this photocathode, (f) Variation of the yield rate of formate (circles) and hydrogen (squares) on Ru(bpy)$_2$dppz-Co_3O_4/CA with the applied potentials [198]. Reproduced with permission: Copyright 2016, Royal Society of Chemistry.

surface (Fig. 13e and f). They also explained why the main product is methanol in electrolyte and why the reaction and/or diffusion process can control the overpotential.

5.3. *Surface reaction*

Surface reaction is an important step in the process of photoelectrocatalysis. After generating electron/hole pairs, they need to be separated and transferred to the catalyst surface to carry out redox reaction. The adsorption of CO_2 on the active sites on catalyst is very important, which is the basis of starting catalytic CO_2 reduction reaction. Therefore, enhancing CO_2 adsorption can effectively improve the efficiency of photoelectrocatalytic CO_2 reduction. Additionally, CO_2 is a stable nonpolar linear molecule, which is difficult to be directly reduced. Enhancing the activation of CO_2 on photoelectrocatalyst can reduce the reaction barrier and improve reduction efficiency of CO_2. Moreover, activation of CO_2 also can affect the reaction pathway to determine product selectivity of photoelectrocatalytic CO_2 reduction. In photoelectrocatalytic CO_2 reduction, various intermediates or byproducts can be obtained. Notably, the adsorption and desorption of intermediate or byproducts can also affect the selectivity of target product. The section will discuss the effects of surface reaction on photoeletrocatalytic CO_2 reduction and also summarized how to control the surface reaction of catalyst to enhance the photoelectrocatalytic performance.

5.3.1. *Adsorption and activation of reactants*

Generally, the main reactants include CO_2 and H_2O in photocatalytic CO_2 reduction. CO_2 is a stable nonpolar linear molecule and the bond energy C=O is 799 kJ mol^{-1}, which determine the activation and direct reduction of CO_2 is difficult [186]. Enhancing adsorption and activation

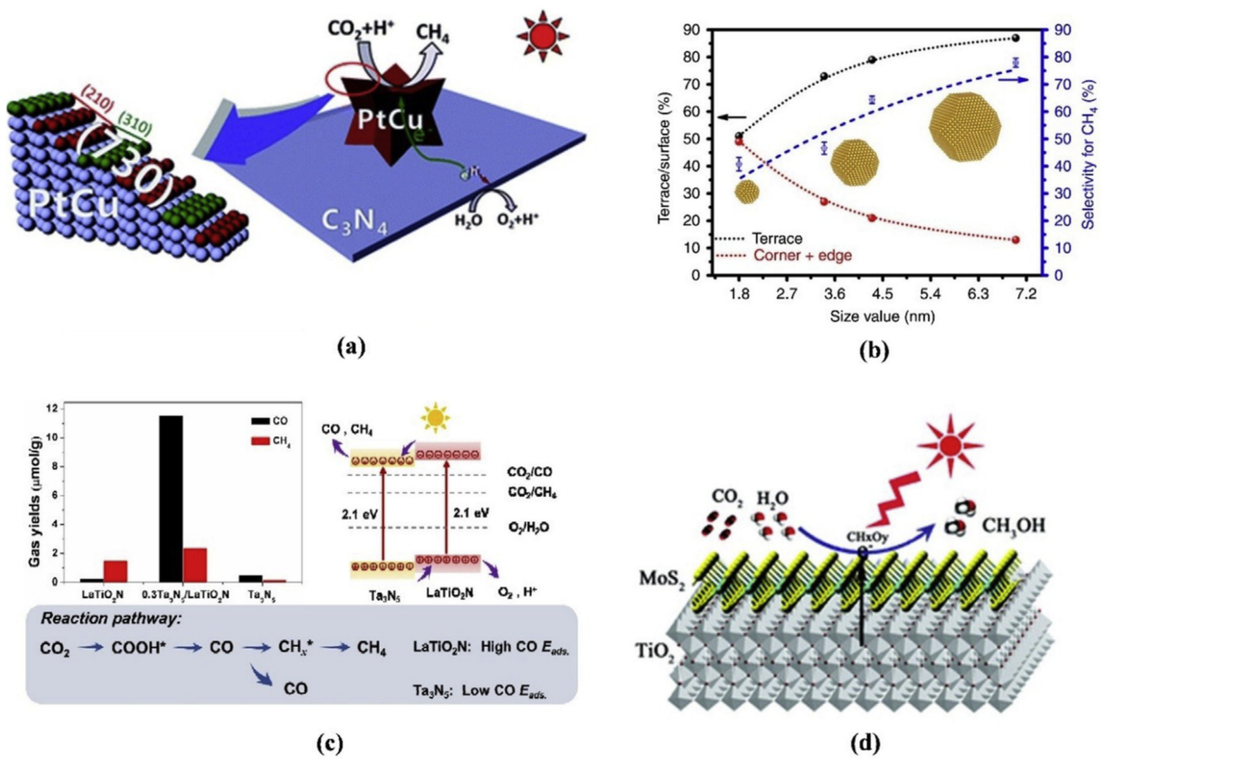

Fig. 15. (a) The high-index (730) facets of PtCu co-catalysts on C_3N_4 [203], Reproduced with permission: Copyright 2017, Royal Society of Chemistry. (b) Correlations between CH_4 selectivity and surface site proportion as functions of the size of Pt NPs [39], Reproduced with permission: Copyright 2018, The Author(s). (c) Schematic illustration about the product selection for CO_2 reduction depends on the surface chemistry of Ta_3N_5 and $LaTiO_2N$ photocatalyst [204], Reproduced with permission: Copyright 2018, Royal Society of Chemistry. (d) Mo sites especially Mo-terminated edges on MoS_2 nanosheets benefit the stabilization of intermediate products (CH_xO_y) [205]. Reproduced with permission: Copyright 2017, Royal Society of Chemistry.

of CO_2 on photocathode can improve CO_2 utilization efficiency and reduce reaction barrier, which greatly affects product selectivity [187]. Adjusting the coordination modes with CO_2 by changing the surface atomic construction of photocathode can significantly enhance adsorption and activation of CO_2 [87]. In addition, H_2O not only consumes photogenerated holes to undergo oxidation half-reaction but also provides proton source for CO_2 hydrogenation process [64,188]. Moreover, H_2O can affect the adsorption structures of CO_2 on catalyst surface due to the co-adsorption of H_2O and CO_2 [189]. Therefore, enhancing adsorption activation of CO_2 and balancing the competitive adsorption of H_2O and CO_2 are the key to determine the reaction efficiency and product selectivity of CO_2 reduction [87,189–195]. And for photoelectrocatalytic CO_2 reduction system with two electrode chambers mentioned in Fig. 1, the H_2O oxidation and CO_2 reduction are carried out in anode chamber and cathode chamber, respectively. Therefore, the competitive adsorption of H_2O and CO_2 would be obviously inhibited. The key of regulating the reaction efficiency and product selectivity of photoelectrocatalytic CO_2 reduction is to enhance the adsorption and activation of CO_2. Cardoso et al. [196] reported a Ti/TiO_2 nanotubes by zeolite imidazole framework-8 (ZIF-8) for photoelectrocatalytic CO_2 reduction to alcohols (Fig. 14a). The experiment results exhibited the increased photocurrent of ZIF-8 at Ti/TiO_2 electrodes. And the concentration of CO_2 was dramatically increased in saturated solution with CO_2, which indicated the efficient preconcentration of CO_2 on the electrode. When CO_2 adsorbed on ZIF-8, the nitrogenated sites of the imidazolate groups in the ZIF-8 complex would interact with CO_2 (Fig. 14b) to form stable carbamates, which promoted the adsorption and activation of CO_2. Under light irradiation, photoelectrocatalytic efficiency of CO_2 reduction to form alcohols was greatly improved. Under UV–vis irradiation and an external potential, the formation mechanism of alcohol on Ti/TiO_2NT-ZIF-8 electrodes was proposed in Fig. 14b.

Additionally, Shen et al. [197] constructed a biomimetic photoelectrocatalytic interface. The cobalt-containing zeolite imidazolate framework (ZIF9) acts as CO_2 fixation and activation substrate, and Co_3O_4 nanowires (NWs) performs as the photoelectrocatalyst. For ZIF9 modified Co_3O_4 NWs, CO_2 could be concentrated on ZIF9 and activated via binding Co atom to the O atom of CO_2 (Fig. 14c). By photoelectrochemical CO_2 conversion, formate was produced with conversion rate (72.3 $\mu mol \cdot L^{-1} \cdot cm^{-2} \cdot h^{-1}$) and selectivity (~100%) at a low overpotential of 290 mV. The proposed mechanism of photoelectrocatalytic CO_2 reduction on ZIF9-Co_3O_4 NWs was shown in Fig. 14d. Moreover, Huang et al. [198] established a photoelectrocatalytic interface with semiconductor/metal-complex hybrid, which can enhance adsorption and activation of CO_2 by using a carbon aerogel as the CO_2 fixation substrate. Compared the CO_2 surface concentration on Co_3O_4/FTO, that in this hybrid interface has a 380-fold increase. The photoeletrocatalytic mechanism of CO_2 reduction was exhibited in Fig. 14e, CO_2 was firstly activated to form $CO_2^{\bullet-}$ and then turned into $HCOO^-$ by protonation, conversing to the formate in the end. The yield of formate reached at 110 $\mu mol \cdot cm^{-2} h^{-1}$ (Fig. 14f) with a selectivity of 99.95%.

5.3.2. Active sites and adsorption/desorption of intermediates

The intrinsic properties of active sites would determine their practicability for different target catalytic reactions, which makes the product selectivity is closely related to the number and type of active sites [199]. Therefore, designing and regulating active sites can effectively adjust product selectivity of CO_2 reduction [51,87,200–202]. The low coordinated atoms on surface of catalyst can generally perform as good active sites to activate CO_2 and promote reaction. And the high-index facets may form more low coordinated atoms. For example, Lang et al. [203] found the high-index (730) facets of PtCu co-catalysts showed better improvement effect on generating efficiency and selectivity of CH_4 than

Table 1
Some photo-electrocatalytic systems reported for the CO_2 reduction.

Electrode	Efficiency[a)]	Conditions[b)]	Ref.
Type I: photocathode + dark anode			
Photocathode: Cu_2O|AF-PSi Anode: Stainless steel sheet	HCOOH, FE:61%	HAL-320 (Asahi Spectra), 1 Sun, 2 h 0.2 M Na_2SO_4, −0.3 V (*vs.* Ag | AgCl)	[209]
Photocathode: 5% PANI@$CuFe_2O_4$ Anode: Pt	Methanol: 33.7 mmol/L.cm^2 FE: 73%	Visible light, 4 h, −0.4 V *vs.* NHE	[210]
Photocathode: Co_3O_4 Microbial anode	HCOOH: 239 μmol	150 W Xe lamp (380–780 nm), 10 h, 0.1 M Na_2SO_4, resistance (300 Ω)	[211]
Photocathode: Au–TiO_2/GaN/ n^+-p Si Anode: Pt	CO, FE:56%	AM1.5G, 0.5 M $KHCO_3$, 100 min, +0.17 V *vs.* RHE	[212]
Photocathode: Cu/ *p*-NiO Anode: Pt	CO and $HCOO^-$, FE: account for 50% of total FE from the device	high-power LEDs, 50 mM K_2CO_3, −0.7 V_{RHE} (V *vs.* RHE)	[213]
Photocathode: CoPc/CNT-C-$CsFAPb(IBr)_3$ Anode: graphite plate	CO, FE: 68.4%–87.5%	AM 1.5G, 0.5 M $KHCO_3$, 0.47 V–0.17 V *vs.* RHE	[214]
Photocathode: $Cu_2O/CuFeO_2$ Anode: Pt	Formate, FE: 21.6%, Acetate, FE: 68.6%	300W Xe lamp (100 mW/ cm^2), 0.5 M $KHCO_3$, 0.35 V *vs.* RHE, 30min	[215]
Photocathode: Si/ Bi5 Anode: Pt	Formate, FE: 73.0%	AM 1.5G, 0.5 M $KHCO_3$, −1.43 V *vs.* RHE,30min	[216]
Photocathode: Ti/ TiO_2NT-$Ru_3(BTC)_2$ Anode: DSA®	Methanol: 314 μmol/ L	UV–vis light, 0.1 mol L^{-1} Na_2SO_4, -0.5 V *vs.* Ag/ AgCl, 3 h	[217]
Photocathode: Si NW/Ni SA Bioanodes	CO, FE: ~80%, Tunable CO:H_2 ratio: (0.1–6.8)	1 sun illumination, 0.25 M $KHCO_3$, 0.24 V *vs.* RHE	[218]
Photocathode: Ti/ TiO_2NT@PDA-AgNP Anode: DSA®	Methanol, FE:78%	UV–vis light, 0.1 M Na_2SO_4, −0.7 V vs. Ag/AgCl	[219]
Photocathode: $Zn_{0.5}$CZGS_540 Anode: Pt	CO: 0.28 μmol, FE: 3.3% H_2:6.8 μmol, FE: 80.0%	AM 1.5G, 0.1 M $KHCO_3$, 1.5 h–2h,	[220]
Photocathode: NiO|Si-Poly(RuII)-Poly(ReI) Anode: Pt	CO: 1248 nmol, FE:65% TON_{CO}:58	Visible light (100 mW/ cm^2), 10 h, 50 mM $NaHCO_3$, -0.7 V vs. Ag/ AgCl	[221]
Photocathode: a-Si/TiO_2/Au Anode: Pt	CO/H_2 ratios: 1:2 to 1:3.1(ST-4Au), CO/H_2 ratios: 1:1 (ST-7Au)	AM 1.5G (100 mW/cm^2), 0.1 M $KHCO_3$,	[222]
Photocathode: Si with Ag-supported dendritic Cu catalysts Anode: IrO_2	C_2–C_3 products, FEs: 70%	AM 1.5G, 0.1 M $CsHCO_3$, −0.4 *vs.* RHE	[223]
Photocathode: NiO/QD/Re Anode: Pt	CO, FE:32% TON: 11	Visible light (LED), 0.1 M $AgNO_3$ in acetonitrile, −0.87 V *vs.* NHE	[224]
Photocathode: Cu-MOF/Cu_2O Anode: Pt	CO, FE: 95%	AM 1.5G, 1 h, between −1.77 and −1.97 V vs Fc/ Fc^+, 0.1 M tetrabutylammonium hexafluorophosphate	[71]
Photocathode: Si | *n*-GaN | -NPhN-$Ru(CP)_2^{2+}$-RuCt Anode: Pt	Formate, FE:64%	AM 1.5G, 20 h, 50 mM $NaHCO_3$, −0.25 V *vs.* RHE,	[169]
			[225]

Table 1 (*continued*)

Electrode	Efficiency[a)]	Conditions[b)]	Ref.
Photocathode: $CuFe_2O_4$ Anode: Pt/C	Methanol, FE: 62% Quantum efficiency:14.4%	Visible light, 0.1 M $NaHCO_3$, −0.50 V *vs.* NHE	
Photocathode: Cu_2O/TiO_2–Cu^+ Anode: Pt	Methanol, FE: 56.5%	AM 1.5G, 0.3 M $KHCO_3$, 0.3 V (*vs.* RHE)	[226]
Photocathode: n^+ *p*-Si/Sn-pNWs Anode: Pt	HCOOH, FE: ~60%	AM 1.5G, 0.1 M $KHCO_3$, −0.4 V *vs.* RHE	[143]
Photocathode: $CuFeO_2$/CuO Anode: Pt	Acetate, FE: 80%, Formate	Visible light, 2 h 0.1 M $KHCO_3$, −0.4 V *vs.* Ag/AgCl	[227]
Photocathode: Au–TiO_2 NTPC/ Cu NPs Anode: graphite	HCOOH: 1019.3 μmol L^{-1} cm^{-2}, FE: 82.6%	AM1.5 G, 6 h 0.1 M $NaHCO_3$, −1.0 V *vs.* Ag/AgCl,	[228]
Photocathode: Co_3O_4 NWs/ZIF9 Anode: Pt	Formate: 578.8 μmol L^{-1} cm^{-2}, FE: 70.5%	Xenon lamp, 8 h 0.1 M Na_2SO_4, −0.9 V *vs.* SCE,	[229]
Photocathode: Si NWs/Au_3Cu NPs Anode: Pt	CO, FE: 80%	AM1.5 G, 3 h 0.1 M $KHCO_3$, −0.2 V *vs.* RHE	[230]
Photocathode: Co_3O_4/ $Ru(bpy)_2dppz$ Anode: graphite plate	Formate: 110 mmol cm^{-2} h^{-1}, FE: 86%	Visible light, 8 h, 0.1 M $NaHCO_3$, −0.6 V vs NHE,	[198]
Type II: dark cathode + photoanode			
Cathode: MPc-GDE Photoanode: TiO_2	CO, FE: 98%	Hg lamp, 3 h, 0.1 M Na_2SO_4, −0.8 V vs. Ag/AgCl	[231]
Cathode: CoO_x Photoanode: TNTs	Formic acid: 56.6 μmol/(cm^2·h)	300 W Xe lamp, 1 h, 0.5 mol/L Na_2SO_4, 0.6 V (*vs.* Ag/AgCl)	[232]
Biocathode: CHT/ Ni Foam Photoanode: FTO/ $BiVO_4$/Mo	Acetate, 6.42 ± 1.21 mM FE: 62 ± 12%, Solar-to-acetate efficiency: 0.97 ± 0.19%	AM 1.5G (50 mW/cm^2), 7d, −0.72 ± 0.03 V vs. SHE	[233]
Biocathode Photoanode: TiO_2/ CdS	CH_4, FE: 94.4%, Solar-to-fuel efficiency: 1.28%	AM 1.5G, 6d, No external bias, 0.35 M Na_2SO_3 and 0.25 M $Na_2S\cdot 9H_2O$	[234]
Cathode: Cu mesh electrode Photoanode: TCN/ TiO_2	HCOOH: 110 ± 10 μmol/h, selectivity of ca. 51.7%.	50 W LED light, 0.5 M $KHCO_3$, 1.2 V_{RHE}	[235]
Cathode: Cu Photoanode: TiO_2-based MEA	Methanol: 9.5 μmol m^{-2} s^{-1}, FE: 16.2%, Ethanol: 6.8 μmol m^{-2}·s^{-1}, FE: 23.2%	UV LED light (100 mW cm^{-2}), −1.8 V *versus* Ag/AgCl	[236]
Cathode: CuZn-0.5 Photoanode: $BiVO_4$	HCOOH, FE:60%	Simulated sunlight, −1.1 V vs RHE, 0.1 M $KHCO_3$ (cathodic), 0.1 M $KHCO_3$-0.05 M Na_2SO_3 (anodic)	[237]
Cathode: Pt Photoanode: Co-Pi/ $BiVO_4/SnO_2$ NSA	CO, maximum FE: 90.0%,	AM 1.5G, 1.1 V, 0.5 M Potassium phosphate buffer	[238]
Cathode: Pt Photoanode: 0.4CdS	CO: 316 μmol·g^{-1}·h^{-1},	visible light, 0.1 M $KHCO_3$, −0.3 V *vs.* Ag/AgCl	[239]
Cathode: Cu/Cu_2O Photoanode: TiO_2	CH_3OH, FE: 53.6%	AM 1.5G, 0.1 M $KHCO_3$, 0.75 V vs. RHE	[240]
Cathode: Indium Photoanode: WO_3	Formic acid: 9.21 mmol h^{-1} cm^{-2}, FE: 45.45%	AM 1.5G, 3 h 0.2 M Na_2SO_4(anodic), 0.5 M $KHCO_3$ (cathodic), 1.2 V (*vs.* Ag/AgCl)	[241]
Cathode: IO-TiO_2| FDH Photoanode: IO-TiO_2|dpp| POs–PSII	Formate, FE: 78 ± 8%	AM 1.5G, 100 mM $NaHCO_3$, −0.6 V *vs.* SHE	[242]

(*continued on next page*)

Table 1 (*continued*)

Electrode	Efficiency[a)]	Conditions[b)]	Ref.
Cathode: Cu foam Photoanode: Sn-WO_3	HCOOH: 485 nmol cm^{-2}; IPCE: 45.1%	Visible light, 3 h 0.5 M $KHCO_3$, 0.8 V *vs.* Ag/AgCl,	[243]
Cathode: Pt Photoanode: B-WO_3(002)	HCOOH, IPCE: 66.7%	AM1.5 G, 3 h, 0.2 M Na_2SO_4, 0.6 V vs Ag/AgCl	[244]
Cathode: MWCNTs/CoII(Ch) Photoanode: $BiVO_4$/FeOOH	CO, FE: 83%	AM1.5 G, 50 h, 5.0×10^{-3}M Na_2SO_4, −1.3 V *vs.* cathode,	[245]
Cathode: Pd/C–Ti mesh Photoanode: GaAs/InGaP/TiO_2/Ni	Formate; FE: 94%	AM1.5 G, 3 h, 1.0 M KOH + 2.8 M $KHCO_3$, 8.5 mA cm^{-2}	[246]
Cathode: EC-PDA Photoanode: $BiVO_4$/CoPi	Formate, FE: 99.2%	AM1.5 G, 24 h, 0.1 M Na phosphate buffer, no bias	[247]
Cathode: Pd_7Cu_3 Photoanode: CNTs/ZnO/Co_3O_4 NW	CO, FE: 75%	AM1.5 G, 4 h, 0.1 M K_2SO_4 + 0.1 M $KHCO_3$, −1.3 V *vs.* cathode	[248]
Type III: photocathode + photoanode			
Photocathode: CoPc/CNT-C-$CsFAPb(IBr)_3$ Photoanode: IrO_x/a-Si	CO, FE:83%, H_2, FE: 14%	AM 1.5G, No external bias 0.5 M $KHCO_3$, 20 h	[214]
Photocathode: *p*-GaN/AuNPs/RuCY Photoanode: α-Fe_2O_3/FTO	HCOOH, FE: 96.8 %, Selectivity: 98.2%	AM 1.5G, 20 h, 0.2 M phosphate buffer −1.05 V_{RHE}	[249]
Photocathode: TiO_2 Photoanode: $BiVO_4$	Methanol: 55.5 $\mu M\cdot h^{-1}\cdot cm^{-2}$	300 W Xe lamp (100 mW/cm^2), 0.1 M $NaHCO_3$, 0.6 V vs. Ag/AgCl	[250]
Photocathode: Mn: CdS-CST-TiO_2 Photoanode: NiOOH/FeOOH/$BiVO_4$	Methanol: 90 $\mu M\cdot h^{-1}cm^{-2}$,	Xe lamp, 0.1 M [APMIm]Br ILs	[251]
Photocathode: $BiFeO_3$ Photoanode: Co-Pi/α-Fe_2O_3	CH_3OH: 220 μmol h^{-1}	AM 1.5G, 6 h, 0.8 V, 50 × 10^{-3} M phosphate buffer	[252]
Photocathode: H–SiNW Photoanode: 3-jn-Si/ITO/CoPi	Formate: 0.26 × 10^{-3} M; FE: 16.18%	Visible light, 50 × 10^{-3} M phosphate buffer, 1.8 V, 6 h	[253]
Photocathode: Si NWs@CoN/CN Photoanode: TiO_2 NWs@CoP/CN	CO, FE: 73%	Visible light, 0.5 M H_2SO_4, 1 M KOH, −0.2 V *vs.* RHE, 8 h	[254]
Type IV: (photo)cathode + solar cell			
Cathode: Au Solar cell: perovskite photovoltaics Anode: IrO_2	CO, FE: exceeding 90%	AM 1.5G, 2 h, 0.5 M $NaHCO_3$, −0.4 V vs. RHE	[76]
Photocathode: BCW-X Solar cell: Si Photoanode: $BiVO_4$	Ethanol: 11.4 $\mu M\cdot h^{-1}\cdot cm^{-2}$ (600 $\mu mol\cdot h^{-1}\cdot g^{-1}$), Selectivity: 80.0%	300W Xe lamp, 2 h, 0.1 M $KHCO_3$, −1.0 V	[255]
Photocathode: ZnO/ZnTe/CdTe/Au Perovskite solar cell: $CH_3NH_3PbI_3$ Anode: Co-Ci	CO: 35 μmol	AM1.5 G, 3 h, 0.5 M $KHCO_3$, no bias	[256]
Photocathode: GaN NW-silicon solar cell Anode: Pt	CH_3OH: 25.5 mmol h^{-1} cm^{-2}, FE: 19%	AM1.5 G, 100 min, 0.5 M $KHCO_3$, −1.4 V *vs.* Ag/AgCl,	[257]
Type V: continuous-flow system			
Cathode: Ag nanocubes Photoanode: WO_3/$BiVO_4$	CO, FE: 92.1%	AM1.5G, 4 h, 1.4 V *vs.* Ag/AgCl	[81]

a) Including the reduction product amounts, concentrations, or rates, turnover number (TON) and/or Faradaic efficiency (FE); b) Including light source, electrolyte, applied potential, and/or reaction time.

low-index (100) facets. Which might be attributed to the formation of more low-coordinated metal active sites in high-index (730) facets (Fig. 15a). Moreover, the surface structure of catalyst will be greatly affected by size and might induce the formation of different active sites on surface, which can significantly determine product selectivity of CO_2 reduction. For instance, Dong et al. [39] studied the size effect of Pt NP co-catalysts for CO_2 reduction. The selectivity of CH_4 shows a consistent trend with the terrace site fraction but shows the opposite relationship with the low-coordinated site fraction over the variously sized Pt NPs (Fig. 15b). Therefore, they conjectured that the active sites were terrace sites to generate CH_4 on Pt NPs while the low-coordinated sites might be active sites to hydrogen evolution. The structure of semiconductor photoelectrode is essentially similar to that of photocatalyst or electrocatalyst, so the construction and design of active sites on photoelectrode to control the efficiency and selectivity of CO_2 reduction can actually find inspiration from the cases of photocatalysis or electrocatalysis. At present, the research progress on the construction of active sites in photoelectrocatalytic CO_2 reduction is relatively slow and insufficient, and the typical cases of active site design in photocatalyst or electrocatalyst can guide and develop the design of photoelectrodes with unique active sites. According to the above analysis, it might be feasible that the efficiency and selectivity of photoelectrocatalytic CO_2 reduction could be effectively improved by constructing suitable active sites on photoelectrode. This is also an important research direction of photoelectrocatalytic CO_2 reduction.

Additionally, many kinds of intermediates or byproducts can be obtained during the process of CO_2 reduction. The adsorption and desorption of intermediate or byproducts would influence on the target product selectivity. If the interaction between intermediate and catalyst is strong, it may be difficult for the intermediate to desorb from the catalyst surface, which makes further hydrogenation reduction reaction more possible. On the contrary, the weak interaction would lead to easier desorption and release from the surface of catalyst for byproducts, which might greatly affect the active site exposure and product selectivity [87, 204–208]. For example, the adsorption and desorption properties of CO, as an important intermediate, would significantly determine the product selectivity in photocatalytic CO_2 reduction [204,206,207]. Lu et al. [204] reported that the weak adsorption of CO on the surface of Ta_2N_5 leaded to the rapid desorption of CO, which became the main product on Ta_3N_5. However, CO can strongly adsorb on the surface of $LaTiO_2N$, which made CH_4 become the final product. Besides CO, the adsorption properties of the methoxy ($\cdot OCH_3$ and $\cdot CH_3$) radicals and CH_xO_y intermediates also greatly influence on product selectivity of photocatalytic CO_2 reduction [205,208]. For example, Tu et al. [205] reported that CO_2 can selectively reduce to form CH_3OH on MoS_2-modified TiO_2 (Fig. 15d). During photocatalytic CO_2 reduction, the Mo sites can stabilize CH_xO_y intermediates by electrostatic attraction, which is beneficial to selectively reduce CO_2 to form CH_3OH. For photoelectrocatalytic CO_2 reduction on semiconductor photoelectrode, the conversion process of CO_2 is similar to that on semiconductor photocatalyst, which means that the adsorption and desorption of intermediate also can determine product selectivity. According to above discussions, there is a strong correlation between active sites and adsorption/desorption of intermediates. Therefore, when designing and constructing the active sites, it is necessary to comprehensively consider the effects on adsorption/desorption of the intermediates, enhancing product selectivity in photoelectrocatalytic CO_2 reduction.

6. Some reported PEC CO_2 reduction system application

Up to now, various photoelectrocatalysts have been reported to be used in typical systems of photoelectrocatalytic CO_2 reduction (Figs. 1 and 2) and Table 1 summarized the detailed experimental conditions and obtained efficiencies as follows. Generally, photoeletrocatalytic CO_2 reduction is carried out in a three-electrode system including work electrode, counter electrode and reference electrode. Additionally, light source, electrolyte and applied bias voltage are usually used as reference for basic experimental conditions. According to the reported results, the most evaluation parameters of efficiency include Faraday efficiency (FE), product conversion rate or current density. And a few results calculated the turnover number (TON) or quantum yield (QY). In fact, there is still no standard test specification, which make it difficult to reliably compare the results of different laboratories. We recommend the evaluation parameters discussed in the third part of this paper, which integrated the efficiency evaluation of electrocatalysis and photocatalysis. Moreover, the CO_2 reduction reaction on photoelectrode is very complex involving the adsorption-conversion-desorption of intermediates. Therefore, the reaction stability of the photoelectrode is very important for the practical application of photoelectrocatalytic CO_2 reduction and a stability test is needed in the experiments. Although various kinds of photoelectrocatalytic materials have been developed for CO_2 reduction, they are basically in the laboratory research stage and far from practical application.

7. Summary and prospect

With development of society and increase of world population, the demand for energy is soaring year by year. Among various applications, solar-driven CO_2 reduction to generate low-carbon fuels or small-molecule organic compounds not only benefits CO_2 emission reduction, but also can be used as a carrier of energy storage to some extent, which is significant to alleviate energy shortage and global environmental crisis. Among diversiform methods for CO_2 conversion, the photoelectrocatalysis can endow more remarkable performance by integrating photocatalysis with electrocatalysis and developing the merits of both approaches. In recent years, the photoelectrocatalytic CO_2 reduction developed rapidly, which have been systematically summarized and discussed in this review.

To better understand the principle of photoelectrocatalysis, technical principles of photocatalysis and electrocatalysis were firstly summarized and expounded, respectively, and their advantages and disadvantages were compared. Then the main system and principle of photoelectrocatalysis are summarized. According to the different materials of photoelectrode, the photoelectrocatalytic CO_2 reduction system can be divided into following categories: I. dark anode and *p*-type photocathode, II. dark cathode and *n*-type photoanode, III. *p*-type photocathode and *n*-type photoanode. Recently, some novel system have been also developed to carry out photoeletrocatalytic CO_2 reduction. Ⅳ, a novel tandem device is developed by integrating a solar cell for supplying external voltage to promote CO_2 reduction reaction, also showing the excellent efficiency and promising potential. Ⅴ, a continuous-flow PEC CO_2 reduction system was also developed, which directly introduce gas CO_2 onto the surface of cathode to carry out reduction reaction, showing excellent selectivity. Then, the influence factors of photoelectrocatalytic CO_2 reduction were also discussed and analyzed, including influence of photoelectrode (thermodynamics and kinetics), interaction between reaction molecules and catalysts (initial activation and C–C bond formation), reaction conditions (such as light source, electrolyte effect and overpotential, etc.). Notably, enhancing the product selectivity in the reaction process of photoelectrocatalytic CO_2 reduction is one of the keys to obtain high yield of target product and realize practical application. Considering that the structure and reaction characteristics on photoelectrode are the key factors affecting the efficiency and selectivity of photoelectrocatalytic CO_2 reduction, we discussed the main strategies for enhancing the reaction efficiency and product selectivity of photoelectrocatalytic CO_2 reduction on photoelectrode include photoexcitation (e.g., doping element, introducing surface plasmon and quantum dots), charge separation efficiency (e.g., loading co-catalysts, constructing heterojunction and defect structure), surface reaction (e.g., adsorption and activation of reactants, adsorption/desorption of intermediates), and their synergistic effects.

Although these strategies have been made in enhancing reaction efficiency and product selectivity of CO_2 reduction, many explorations and approaches are still in the initial stage, which leads to a fact that realizing large-scale practical applications still need a long way to go. Some typical challenges and issues are listed below: (1) the conversion efficiency and product selectivity of CO_2 are still insufficient for practical application; (2) the comprehensive and reliable detection system and standard is lacking; (3) developing more advanced *in-situ* characterizations to reveal reaction mechanism and conversion pathway is necessary; (4) combining with DFT calculation and experiment is powerful to guide the design of photoelectrocatalyst. Although challenges and hidden dangers still exist in this field, we believe optimistically that the technology of photoeletrocatalytic CO_2 reduction can realize the practical application. With the further development and combination of experiment and computation to deeply explore conversion mechanism, novel and efficient photoelectrocatalytic CO_2 reduction systems will be designed to accommodate large-scale applications in the near future.

Declaration of competing interest

None.

Acknowledgement

This work was supported by the National Natural Science Foundation of China (Grant Nos. 21822601, 21777011, and 52002054), the Fundamental Research Funds for the Central Universities (ZYGX2019Z021), the 111 Project (B20030), and the Plan for "National Youth Talents" of the Organization Department of the Central Committee.

References

[1] S. Zhao, R. Jin, R. Jin, Opportunities and challenges in CO_2 reduction by gold- and silver-based electrocatalysts: from bulk metals to nanoparticles and atomically precise nanoclusters, ACS Energy Lett. 3 (2018) 452–462.
[2] L. Yu, Y. Xie, J. Zhou, Y. Li, Y. Yu, Z. Ren, Robust and selective electrochemical reduction of CO_2: the case of integrated 3D TiO_2@MoS_2 architectures and Ti–S bonding effects, J. Mater. Chem. A 6 (2018) 4706–4713.
[3] T. Yu, Y. Chen, Effects of elevated carbon dioxide on environmental microbes and its mechanisms: a review, Sci. Total Environ. 655 (2019) 865–879.
[4] Z. Zhang, S.-Y. Pan, H. Li, J. Cai, A.G. Olabi, E.J. Anthony, V. Manovic, Recent advances in carbon dioxide utilization, Renew. Sustain. Energy Rev. 125 (2020), 109799.
[5] C. Graves, S.D. Ebbesen, M. Mogensen, K.S. Lackner, Sustainable hydrocarbon fuels by recycling CO_2 and H_2O with renewable or nuclear energy, Renew. Sustain. Energy Rev. 15 (2011) 1–23.
[6] S.C. Peter, Reduction of CO_2 to chemicals and fuels: a solution to global warming and energy crisis, ACS Energy Lett. 3 (2018) 1557–1561.
[7] W. Zhang, A.R. Mohamed, W.-J. Ong, Z-scheme photocatalytic systems for carbon dioxide reduction: where are we now? Angew. Chem. Int. Ed. 59 (2020) 22894–22915.
[8] L. Wang, Y. Yi, H. Guo, X. Tu, Atmospheric pressure and room temperature synthesis of methanol through plasma-catalytic hydrogenation of CO_2, ACS Catal. 8 (2018) 90–100.
[9] C. Wang, X. Chen, H. Pan, D. Qi, J. Jiang, Towards developing efficient aminopyridine-based electrochemical catalysts for CO_2 reduction. A density functional theory study, J. Catal. 373 (2019) 75–80.
[10] S. Cao, B. Shen, T. Tong, J. Fu, J. Yu, 2D/2D heterojunction of ultrathin MXene/Bi_2WO_6 nanosheets for improved photocatalytic CO_2 reduction, Adv. Funct. Mater. 28 (2018), 1800136.
[11] D. Ješić, D. Lašič Jurković, A. Pohar, L. Suhadolnik, B. Likozar, Engineering photocatalytic and photoelectrocatalytic CO_2 reduction reactions: mechanisms, intrinsic kinetics, mass transfer resistances, reactors and multi-scale modelling simulations, Chem. Eng. J. 407 (2021), 126799.

[12] N.M. Martin, P. Velin, M. Skoglundh, M. Bauer, P.-A. Carlsson, Catalytic hydrogenation of CO_2 to methane over supported Pd, Rh and Ni catalysts, Catal. Sci. Technol. 7 (2017) 1086–1094.
[13] Y.Y. Birdja, E. Pérez-Gallent, M.C. Figueiredo, A.J. Göttle, F. Calle-Vallejo, M.T.M. Koper, Advances and challenges in understanding the electrocatalytic conversion of carbon dioxide to fuels, Nat. Energy 4 (2019) 732–745.
[14] R.-B. Song, W. Zhu, J. Fu, Y. Chen, L. Liu, J.-R. Zhang, Y. Lin, J.-J. Zhu, Electrode materials engineering in electrocatalytic CO_2 reduction: energy input and conversion efficiency, Adv. Mater. 4 (2019), 1903796.
[15] J. Wu, Y. Huang, W. Ye, Y. Li, CO_2 reduction: from the electrochemical to photochemical approach, Adv. Sci. 4 (2017), 1700194.
[16] Y. Zhou, Z. Wang, L. Huang, S. Zaman, K. Lei, T. Yue, Z.a. Li, B. You, B.Y. Xia, Engineering 2D photocatalysts toward carbon dioxide reduction, Adv. Energy Mater. 11 (2021), 2003159.
[17] P. Wang, S. Wang, H. Wang, Z. Wu, L. Wang, Recent progress on photo-electrocatalytic reduction of carbon dioxide, Part. Part. Syst. Char. 35 (2018), 1700371.
[18] P. Ding, T. Jiang, N. Han, Y. Li, Photocathode engineering for efficient photoelectrochemical CO_2 reduction, Mater. Today Nano 10 (2020), 100077.
[19] V. Kumaravel, J. Bartlett, S.C. Pillai, Photoelectrochemical conversion of carbon dioxide (CO_2) into fuels and value-added products, ACS Energy Lett. 5 (2020) 486–519.
[20] S.R. Lingampalli, M.M. Ayyub, C.N.R. Rao, Recent progress in the photocatalytic reduction of carbon dioxide, ACS Omega 2 (2017) 2740–2748.
[21] B. Zhang, L. Sun, Artificial photosynthesis: opportunities and challenges of molecular catalysts, Chem. Soc. Rev. 48 (2019) 2216–2264.
[22] Z. Fu, Q. Yang, Z. Liu, F. Chen, F. Yao, T. Xie, Y. Zhong, D. Wang, J. Li, X. Li, G. Zeng, Photocatalytic conversion of carbon dioxide: from products to design the catalysts, J. CO_2 Util. 34 (2019) 63–73.
[23] X. Wang, J. He, L. Mao, X. Cai, C. Sun, M. Zhu, $CsPbBr_3$ perovskite nanocrystals anchoring on monolayer MoS_2 nanosheets for efficient photocatalytic CO_2 reduction, Chem. Eng. J. (2020), 128077.
[24] V.P. Indrakanti, H.H. Schobert, J.D. Kubicki, Quantum mechanical modeling of CO_2 interactions with irradiated stoichiometric and oxygen-deficient anatase TiO_2 surfaces: implications for the photocatalytic reduction of CO_2, Energy Fuels 23 (2009) 5247–5256.
[25] L. Liu, H. Zhao, J.M. Andino, L. Ying, Photocatalytic CO_2 reduction with H_2O on TiO_2 nanocrystals: comparison of anatase, rutile, and brookite polymorphs and exploration of surface chemistry, ACS Catal. 2 (2012) 1817–1828.
[26] Z. Jiang, W. Sun, W. Miao, Z. Yuan, G. Yang, F. Kong, T. Yan, J. Chen, B. Huang, C. An, G.A. Ozin, Living atomically dispersed Cu ultrathin TiO_2 nanosheet CO_2 reduction photocatalyst, Adv. Sci. 6 (2019), 1900289.
[27] S. Sun, M. Watanabe, J. Wu, Q. An, T. Ishihara, Ultrathin $WO_3{\cdot}0.33H_2O$ nanotubes for CO_2 photoreduction to acetate with high selectivity, J. Am. Chem. Soc. 140 (2018) 6474–6482.
[28] X. Feng, C. Jing, L. Guo, S. Lei, Y. Ni, In situ electrochemically etching-derived ZnO nanotube arrays for highly efficient and facilely recyclable photocatalyst, Appl. Surf. Sci. 258 (2012) 8160–8165.
[29] A.D. Handoko, J. Tang, Controllable proton and CO_2 photoreduction over Cu_2O with various morphologies, Int. J. Hydrogen Energy 38 (2013) 13017–13022.
[30] B. Zhou, J. Song, C. Xie, C. Chen, Q. Qian, B. Han, Mo–Bi–Cd ternary metal chalcogenides: highly efficient photocatalyst for CO_2 reduction to formic acid under visible light, ACS Sustain. Chem. Eng. 6 (2018) 5754–5759.
[31] K. Sasan, Q. Lin, C. Mao, P. Feng, Open framework metal chalcogenides as efficient photocatalysts for reduction of CO2 into renewable hydrocarbon fuel, Nanoscale 8 (2016) 10913–10916.
[32] B. AlOtaibi, S. Fan, D. Wang, J. Ye, Z. Mi, Wafer-level artificial photosynthesis for CO_2 reduction into CH_4 and CO using GaN nanowires, ACS Catal. 5 (2015) 5342–5348.
[33] E.E. Barton, D.M. Rampulla, A.B. Bocarsly, Selective solar-driven reduction of CO_2 to methanol using a catalyzed *p*-GaP based photoelectrochemical cell, J. Am. Chem. Soc. 130 (2008) 6342–6344.
[34] Y. Zhao, G. Chen, T. Bian, C. Zhou, G.I.N. Waterhouse, L.-Z. Wu, C.-H. Tung, L.J. Smith, D. O'Hare, T. Zhang, Defect-rich ultrathin ZnAl-layered double hydroxide nanosheets for efficient photoreduction of CO_2 to CO with water, Adv. Mater. 27 (2015) 7824–7831.
[35] J. Luo, S. Zhang, M. Sun, L. Yang, S. Luo, J.C. Crittenden, A critical review on energy conversion and environmental remediation of photocatalysts with remodeling crystal lattice, surface, and interface, ACS Nano 13 (2019) 9811–9840.
[36] J. Low, J. Yu, W. Ho, Graphene-based photocatalysts for CO_2 reduction to solar fuel, J. Phys. Chem. Lett. 6 (2015) 4244–4251.
[37] Z. Sun, H. Wang, Z. Wu, L. Wang, g-C_3N_4 based composite photocatalysts for photocatalytic CO_2 reduction, Catal. Today 300 (2018) 160–172.
[38] R. Hailili, D.L. Jacobs, L. Zang, C. Wang, Morphology controlled synthesis of $CeTiO_4$ using molten salts and enhanced photocatalytic activity for CO_2 reduction, Appl. Surf. Sci. 456 (2018) 360–368.
[39] C. Dong, C. Lian, S. Hu, Z. Deng, J. Gong, M. Li, H. Liu, M. Xing, J. Zhang, Size-dependent activity and selectivity of carbon dioxide photocatalytic reduction over platinum nanoparticles, Nat. Commun. 9 (2018) 1252.
[40] Z. Xiong, Z. Lei, Y. Li, L. Dong, Y. Zhao, J. Zhang, A review on modification of facet-engineered TiO_2 for photocatalytic CO_2 reduction, J. Photochem. Photobio. C 36 (2018) 24–47.
[41] K. Wang, Q. Li, B. Liu, B. Cheng, W. Ho, J. Yu, Sulfur-doped g-C_3N_4 with enhanced photocatalytic CO_2-reduction performance, Appl. Catal. B Environ. 176–177 (2015) 44–52.
[42] J. Fu, B. Zhu, C. Jiang, B. Cheng, W. You, J. Yu, Hierarchical porous O-Doped g-C_3N_4 with enhanced photocatalytic CO_2 reduction activity, Small 13 (2017), 1603938.
[43] N. Singhal, U. Kumar, Noble metal modified TiO_2: selective photoreduction of CO_2 to hydrocarbons, Mol. Catal. 439 (2017) 91–99.
[44] X. Han, M. Li, Y. Ma, Y. Li, H. Ma, C. Wang, Thermal coupled photocatalysis to enhance CO_2 reduction activities on Ag loaded g-C_3N_4 catalysts, Surf. Interfaces 23 (2021), 101006.
[45] L.-j. Guo, Y.-j. Wang, T. He, Photocatalytic reduction of CO_2 over heterostructure semiconductors into value-added chemicals, Chem. Rec. 16 (2016) 1918–1933.
[46] D.-I. Won, J.-S. Lee, Q. Ba, Y.-J. Cho, H.-Y. Cheong, S. Choi, C.H. Kim, H.-J. Son, C. Pac, S.O. Kang, Development of a lower energy photosensitizer for photocatalytic CO_2 reduction: modification of porphyrin dye in hybrid catalyst system, ACS Catal. 8 (2018) 1018–1030.
[47] X. Jiao, Z. Chen, X. Li, Y. Sun, S. Gao, W. Yan, C. Wang, Q. Zhang, Y. Lin, Y. Luo, Y. Xie, Defect-mediated electron–hole separation in one-unit-cell $ZnIn_2S_4$ layers for boosted solar-driven CO_2 reduction, J. Am. Chem. Soc. 139 (2017) 7586–7594.
[48] X. Wang, K. Li, J. He, J. Yang, F. Dong, W. Mai, M. Zhu, Defect in reduced graphene oxide tailored selectivity of photocatalytic CO_2 reduction on Cs_4PbBr_6 pervoskite hole-in-microdisk structure, Nano Energy 78 (2020), 105388.
[49] A. Wagner, C.D. Sahm, E. Reisner, Towards molecular understanding of local chemical environment effects in electro- and photocatalytic CO_2 reduction, Nat. Catal. 3 (2020) 775–786.
[50] J. Wang, S. Lin, N. Tian, T. Ma, Y. Zhang, H. Huang, Nanostructured metal sulfides: classification, modification strategy, and solar-driven CO_2 reduction application, Adv. Funct. Mater. 31 (2021), 2008008.
[51] Y. Zhang, B. Xia, J. Ran, K. Davey, S.Z. Qiao, Atomic-level reactive sites for semiconductor-based photocatalytic CO_2 reduction, Adv. Energy Mater. 10 (2020), 1903879.
[52] G. Wang, J. Chen, Y. Ding, P. Cai, L. Yi, Y. Li, C. Tu, Y. Hou, Z. Wen, L. Dai, Electrocatalysis for CO_2 conversion: from fundamentals to value-added products, Chem. Soc. Rev. (2021), https://doi.org/10.1039/D0CS00071J.
[53] M.K. Wilsey, C.P. Cox, R.C. Forsythe, L.R. McCarney, A.M. Müller, Selective CO_2 reduction towards a single upgraded product: a minireview on multi-elemental copper-free electrocatalysts, Catal. Sci. Technol. 11 (2021) 416–424.
[54] Y. Wang, Y. Liu, W. Liu, J. Wu, Q. Li, Q. Feng, Z. Chen, X. Xiong, D. Wang, Y. Lei, Regulating the coordination structure of metal single atoms for efficient electrocatalytic CO_2 reduction, Energy Environ. Sci. 13 (2020) 4609–4624.
[55] Y.J. Sa, C.W. Lee, S.Y. Lee, J. Na, U. Lee, Y.J. Hwang, Catalyst–electrolyte interface chemistry for electrochemical CO_2 reduction, Chem. Soc. Rev. 49 (2020) 6632–6665.
[56] S. Popović, M. Smiljanić, P. Jovanovič, J. Vavra, R. Buonsanti, N. Hodnik, Stability and degradation mechanisms of copper-based catalysts for electrochemical CO_2 reduction, Angew. Chem. Int. Ed. 59 (2020) 14736–14746.
[57] L. Sun, V. Reddu, A.C. Fisher, X. Wang, Electrocatalytic reduction of carbon dioxide: opportunities with heterogeneous molecular catalysts, Energy Environ. Sci. 13 (2020) 374–403.
[58] S. Xie, Q. Zhang, G. Liu, Y. Wang, Photocatalytic and photoelectrocatalytic reduction of CO_2 using heterogeneous catalysts with controlled nanostructures, Chem. Commun. 52 (2016) 35–59.
[59] S. Castro, J. Albo, A. Irabien, Photoelectrochemical reactors for CO_2 utilization, ACS Sustain. Chem. Eng. 6 (2018) 15877–15894.
[60] X. Chang, T. Wang, P. Yang, G. Zhang, J. Gong, The development of cocatalysts for photoelectrochemical CO_2 reduction, Adv. Mater. 31 (2019), 1804710.
[61] N. Zhang, R. Long, C. Gao, Y. Xiong, Recent progress on advanced design for photoelectrochemical reduction of CO_2 to fuels, Sci. China Mater. 61 (2018) 771–805.
[62] J. Hu, C. Zhai, M. Zhu, Photo-responsive metal/semiconductor hybrid nanostructure: a promising electrocatalyst for solar light enhanced fuel cell reaction, Chin. Chem. Lett. (2020), https://doi.org/10.1016/j.cclet.2020.09.049.
[63] G. Centi, S. Perathoner, Catalysis: role and challenges for a sustainable energy, Top. Catal. 52 (2009) 948–961.
[64] W. He, X. Wu, Y. Li, J. Xiong, Z. Tang, Y. Wei, Z. Zhao, X. Zhang, J. Liu, Z-scheme heterojunction of SnS_2-decorated 3DOM-$SrTiO_3$ for selectively photocatalytic CO_2 reduction into CH_4, Chin. Chem. Lett. 31 (2020) 2774–2778.
[65] M. Halmann, Photoelectrochemical reduction of aqueous carbon dioxide on *p*-type gallium phosphide in liquid junction solar cells, Nature 275 (1978) 115–116.
[66] T.J. LaTempa, S. Rani, N. Bao, C.A. Grimes, Generation of fuel from CO_2 saturated liquids using a *p*-Si nanowire ‖ *n*-TiO_2 nanotube array photoelectrochemical cell, Nanoscale 4 (2012) 2245, 2240.
[67] S. Ho-Kimura, S.J.A. Moniz, J. Tang, I.P. Parkin, A method for synthesis of renewable Cu_2O junction composite electrodes and their photoelectrochemical properties, ACS Sustain. Chem. Eng. 3 (2015) 710–717.
[68] P. Li, J. Zhang, H. Wang, H. Jing, J. Xu, X. Sui, H. Hu, H. Yin, The photoelectric catalytic reduction of CO_2 to methanol on CdSeTe NSs/TiO_2 NTs, Catal. Sci. Technol. 4 (2014) 1070–1077.
[69] P. Li, H. Wang, J. Xu, H. Jing, J. Zhang, H. Han, F. Lu, Reduction of CO_2 to low carbon alcohols on CuO FCs/Fe_2O_3 NTs catalyst with photoelectric dual catalytic interfaces, Nanoscale 5 (2013) 11748–11754.
[70] J. Zhao, X. Wang, Z. Xu, J.S.C. Loo, Hybrid catalysts for photoelectrochemical reduction of carbon dioxide: a prospective review on semiconductor/metal complex co-catalyst systems, J. Mater. Chem. A 2 (2014) 15228–15233.
[71] X. Deng, R. Li, S. Wu, L. Wang, J. Hu, J. Ma, W. Jiang, N. Zhang, X. Zheng, C. Gao, L. Wang, Q. Zhang, J. Zhu, Y. Xiong, Metal–organic framework coating enhances the performance of Cu_2O in photoelectrochemical CO_2 reduction, J. Am. Chem. Soc. 141 (2019) 10924–10929.

[72] T. Hisatomi, J. Kubota, K. Domen, Recent advances in semiconductors for photocatalytic and photoelectrochemical water splitting, Chem. Soc. Rev. 43 (2014) 7520–7535.
[73] P. Peerakiatkhajohn, J.-H. Yun, H. Chen, M. Lyu, T. Butburee, L. Wang, Stable hematite nanosheet photoanodes for enhanced photoelectrochemical water splitting, Adv. Mater. 28 (2016) 6405–6410.
[74] S. Wang, H. Chen, G. Gao, T. Butburee, M. Lyu, S. Thaweesak, J.-H. Yun, A. Du, G. Liu, L. Wang, Synergistic crystal facet engineering and structural control of WO_3 films exhibiting unprecedented photoelectrochemical performance, Nano Energy 24 (2016) 94–102.
[75] T.J. LaTempa, S. Rani, N. Bao, C.A. Grimes, Generation of fuel from CO_2 saturated liquids using a *p*-Si nanowire ‖ *n*-TiO_2 nanotube array photoelectrochemical cell, Nanoscale 4 (2012) 2245–2250.
[76] M. Schreier, L. Curvat, F. Giordano, L. Steier, A. Abate, S.M. Zakeeruddin, J. Luo, M.T. Mayer, M. Grätzel, Efficient photosynthesis of carbon monoxide from CO_2 using perovskite photovoltaics, Nat. Commun. 6 (2015) 7326.
[77] M. Schreier, F. Héroguel, L. Steier, S. Ahmad, J.S. Luterbacher, M.T. Mayer, J. Luo, M. Grätzel, Solar conversion of CO_2 to CO using Earth-abundant electrocatalysts prepared by atomic layer modification of CuO, Nat. Energy 2 (2017) 17087.
[78] V. Andrei, B. Reuillard, E. Reisner, Bias-free solar syngas production by integrating a molecular cobalt catalyst with perovskite–$BiVO_4$ tandems, Nat. Mater. 19 (2020) 189–194.
[79] K. Li, X. An, K.H. Park, M. Khraisheh, J. Tang, A critical review of CO_2 photoconversion: catalysts and reactors, Catal. Today 224 (2014) 3–12.
[80] D.M. Weekes, D.A. Salvatore, A. Reyes, A. Huang, C.P. Berlinguette, Electrolytic CO_2 reduction in a flow cell, Acc. Chem. Res. 51 (2018) 910–918.
[81] W. Lu, Y. Zhang, J. Zhang, P. Xu, Reduction of gas CO_2 to CO with high selectivity by Ag nanocube-based membrane cathodes in a photoelectrochemical system, Ind. Eng. Chem. Res. 59 (2020) 5536–5545.
[82] D. Giusi, C. Ampelli, C. Genovese, S. Perathoner, G. Centi, A novel gas flow-through photocatalytic reactor based on copper-functionalized nanomembranes for the photoreduction of CO_2 to C1-C2 carboxylic acids and C1-C3 alcohols, Chem. Eng. J. 408 (2021), 127250.
[83] I. Merino-Garcia, E. Alvarez-Guerra, J. Albo, A. Irabien, Electrochemical membrane reactors for the utilisation of carbon dioxide, Chem. Eng. J. 305 (2016) 104–120.
[84] B. Endrődi, G. Bencsik, F. Darvas, R. Jones, K. Rajeshwar, C. Janáky, Continuous-flow electroreduction of carbon dioxide, Prog. Energy Combust. Sci. 62 (2017) 133–154.
[85] J. Durst, A. Rudnev, A. Dutta, Y. Fu, J. Herranz, V. Kaliginedi, A. Kuzume, A.A. Permyakova, Y. Paratcha, P. Broekmann, T.J. Schmidt, Electrochemical CO_2 reduction-A critical view on fundamentals, materials and applications, CHIMIA Int. J. Chem. 69 (2015) 769–776.
[86] J.-P. Jones, G.K.S. Prakash, G.A. Olah, Electrochemical CO_2 reduction: recent advances and current trends, Isr. J. Chem. 54 (2014) 1451–1466.
[87] J. Fu, K. Jiang, X. Qiu, J. Yu, M. Liu, Product selectivity of photocatalytic CO_2 reduction reactions, Mater. Today 32 (2019) 222–243.
[88] S. Xu, E.A. Carter, Theoretical insights into heterogeneous (photo)electrochemical CO_2 reduction, Chem. Rev. 119 (2019) 6631–6669.
[89] W. Tu, Y. Zhou, Z. Zou, Photocatalytic conversion of CO_2 into renewable hydrocarbon fuels: state-of-the-art accomplishment, challenges, and prospects, Adv. Mater. 26 (2014) 4607–4626.
[90] Y. Wang, J. Liu, Y. Wang, A.M. Al-Enizi, G. Zheng, Tuning of CO_2 reduction selectivity on metal electrocatalysts, Small 13 (2017), 1701809.
[91] J. Kou, C. Lu, J. Wang, Y. Chen, Z. Xu, R.S. Varma, Selectivity enhancement in heterogeneous photocatalytic transformations, Chem. Rev. 117 (2017) 1445–1514.
[92] A. Vasileff, C. Xu, Y. Jiao, Y. Zheng, S.-Z. Qiao, Surface and interface engineering in copper-based bimetallic materials for selective CO_2 electroreduction, Inside Chem. 4 (2018) 1809–1831.
[93] Y. Hori, Electrochemical CO_2 reduction on metal electrodes, Mod. Aspect. Electrochem. 42 (2008) 89–189.
[94] Y. Hori, H. Wakebe, T. Tsukamoto, O. Koga, Electrocatalytic process of CO selectivity in electrochemical reduction of CO_2 at metal electrodes in aqueous media, Electrochim. Acta 39 (1994) 1833–1839.
[95] R. Kortlever, I. Peters, S. Koper, M.T.M. Koper, Electrochemical CO_2 reduction to formic acid at low overpotential and with high Faradaic efficiency on carbon-supported bimetallic Pd–Pt nanoparticles, ACS Catal. 5 (2015) 3916–3923.
[96] M.T. Tang, H. Peng, P.S. Lamoureux, M. Bajdich, F. Abild-Pedersen, From electricity to fuels: descriptors for C1 selectivity in electrochemical CO_2 reduction, Appl. Catal. B Environ. 279 (2020), 119384.
[97] J.S. Yoo, R. Christensen, T. Vegge, J.K. Nørskov, F. Studt, Theoretical insight into the trends that guide the electrochemical reduction of carbon dioxide to formic acid, ChemSusChem 9 (2016) 358–363.
[98] A.J. Göttle, M.T.M. Koper, Proton-coupled electron transfer in the electrocatalysis of CO_2 reduction: prediction of sequential *vs* concerted pathways using DFT, Chem. Sci. 8 (2016) 458–465.
[99] Y.Y. Birdja, J. Shen, M.T.M. Koper, Influence of the metal center of metalloprotoporphyrins on the electrocatalytic CO_2 reduction to formic acid, Catal. Today 288 (2017) 37–47.
[100] B.H. Solis, A.G. Maher, D.K. Dogutan, D.G. Nocera, S. Hammes-Schiffer, Nickel phlorin intermediate formed by proton-coupled electron transfer in hydrogen evolution mechanism, Proc. Natl. Acad. Sci. U. S. A 113 (2015), 201521834.
[101] H. Peng, M.T. Tang, X. Liu, P. Schlexer Lamoureux, M. Bajdich, F. Abild-Pedersen, The role of atomic carbon in directing electrochemical $CO_{(2)}$ reduction to multicarbon products, Energy Environ. Sci. 14 (2021) 473–482.
[102] H.Y. Qi Yuan, Miao Xie, Tao Cheng, Theoretical research on the electroreduction of carbon dioxide, Acta Phys. Chim. Sin. 37 (2021), 2010040.
[103] D.A. Torelli, S.A. Francis, J.C. Crompton, A. Javier, J.R. Thompson, B.S. Brunschwig, M.P. Soriaga, N.S. Lewis, Nickel–gallium-catalyzed electrochemical reduction of CO_2 to highly reduced products at low overpotentials, ACS Catal. 6 (2016) 2100–2104.
[104] R. Kortlever, I. Peters, C. Balemans, R. Kas, Y. Kwon, G. Mul, M.T.M. Koper, Palladium–gold catalyst for the electrochemical reduction of CO_2 to C_1–C_5 hydrocarbons, Chem. Commun. 52 (2016) 10229–10232.
[105] K.U.D. Calvinho, A.B. Laursen, K.M.K. Yap, T.A. Goetjen, S. Hwang, N. Murali, B. Mejia-Sosa, A. Lubarski, K.M. Teeluck, E.S. Hall, E. Garfunkel, M. Greenblatt, G.C. Dismukes, Selective CO_2 reduction to C_3 and C_4 oxyhydrocarbons on nickel phosphides at overpotentials as low as 10 mV, Energy Environ. Sci. 11 (2018) 2550–2559.
[106] Q. Fan, M. Zhang, M. Jia, S. Liu, J. Qiu, Z. Sun, Electrochemical CO_2 reduction to C_{2+} species: heterogeneous electrocatalysts, reaction pathways, and optimization strategies, Mater. Today Energy 10 (2018) 280–301.
[107] O.S. Bushuyev, P. De Luna, C.T. Dinh, L. Tao, G. Saur, J. van de Lagemaat, S.O. Kelley, E.H. Sargent, What should we make with CO_2 and how can we make it? Joule 2 (2018) 825–832.
[108] K.J.P. Schouten, Z. Qin, E.P. Gallent, M.T.M. Koper, Two pathways for the formation of ethylene in CO reduction on single-crystal copper electrodes, J. Am. Chem. Soc. 134 (2012) 9864–9867.
[109] K.J.P. Schouten, Y. Kwon, C.J.M.V.D. Ham, Z. Qin, M.T.M. Koper, A new mechanism for the selectivity to C_1 and C_2 species in the electrochemical reduction of carbon dioxide on copper electrodes, Chem. Sci. 2 (2011) 1902–1909.
[110] M. Gattrell, N. Gupta, A. Co, A review of the aqueous electrochemical reduction of CO_2 to hydrocarbons at copper, J. Electroanal. Chem. 594 (2006) 1–19.
[111] F. Calle-Vallejo, M.T.M. Koper, Theoretical considerations on the electroreduction of CO to C_2 species on Cu(100) electrodes, Angew. Chem. Int. Ed. 52 (2013) 7282–7285.
[112] J.H. Montoya, C. Shi, K. Chan, J.K. Norskov, Theoretical insights into a CO dimerization mechanism in CO_2 electroreduction, J. Phys. Chem. Lett. 6 (2015) 2032–2037.
[113] J.D. Goodpaster, A.T. Bell, M. Head-Gordon, Identification of possible pathways for C–C bond formation during electrochemical reduction of CO_2: new theoretical insights from an improved electrochemical model, J. Phys. Chem. Lett. 7 (2016) 1471–1477.
[114] E. Pérez-Gallent, M.C. Figueiredo, F. Calle-Vallejo, M.T.M. Koper, Spectroscopic observation of a hydrogenated CO dimer intermediate during CO reduction on Cu(100) electrodes, Angew. Chem. Int. Ed. 56 (2017) 3621–3624.
[115] T.-T. Zhuang, Y. Pang, Z.-Q. Liang, Z. Wang, Y. Li, C.-S. Tan, J. Li, C.T. Dinh, P. De Luna, P.-L. Hsieh, T. Burdyny, H.-H. Li, M. Liu, Y. Wang, F. Li, A. Proppe, A. Johnston, D.-H. Nam, Z.-Y. Wu, Y.-R. Zheng, A.H. Ip, H. Tan, L.-J. Chen, S.-H. Yu, S.O. Kelley, D. Sinton, E.H. Sargent, Copper nanocavities confine intermediates for efficient electrosynthesis of C3 alcohol fuels from carbon monoxide, Nat. Catal. 1 (2018) 946–951.
[116] D. Ren, N.T. Wong, A.D. Handoko, Y. Huang, B.S. Yeo, Mechanistic insights into the enhanced activity and stability of agglomerated Cu nanocrystals for the electrochemical reduction of carbon dioxide to *n*-propanol, J. Phys. Chem. Lett. 7 (2016) 20–24.
[117] S. Overmans, S. Agustí, Latitudinal gradient of UV attenuation along the highly transparent red sea basin, Photochem. Photobiol. 95 (2019) 1267–1279.
[118] C.-S. Su, S.-M. Yeh, UV attenuation coefficient in water determined by thermoluminescence detector, Radiat. Meas. 26 (1996) 83–86.
[119] H.O.N. Tugaoen, P. Herckes, K. Hristovski, P. Westerhoff, Influence of ultraviolet wavelengths on kinetics and selectivity for N-gases during TiO_2 photocatalytic reduction of nitrate, Appl. Catal. B Environ. 220 (2018) 597–606.
[120] C. Casado, R. Timmers, A. Sergejevs, C.T. Clarke, D.W.E. Allsopp, C.R. Bowen, R. van Grieken, J. Marugán, Design and validation of a LED-based high intensity photocatalytic reactor for quantifying activity measurements, Chem. Eng. J. 327 (2017) 1043–1055.
[121] B. Gayral, LEDs for lighting: basic physics and prospects for energy savings, C. R. Phys. 18 (2017) 453–461.
[122] J.L. White, M.F. Baruch, J.E. Pander, Y. Hu, I.C. Fortmeyer, J.E. Park, T. Zhang, K. Liao, J. Gu, Y. Yan, T.W. Shaw, E. Abelev, A.B. Bocarsly, Light-driven heterogeneous reduction of carbon dioxide: photocatalysts and photoelectrodes, Chem. Rev. 115 (2015) 12888–12935.
[123] K. Hirota, D.A. Tryk, T. Yamamoto, K. Hashimoto, A. Fujishima, Photoelectrochemical reduction of CO_2 in a high-pressure CO_2 + methanol medium at *p*-Type semiconductor electrodes, J. Phys. Chem. B 102 (1998) 9834–9843.
[124] K. Hirota, D.A. Tryk, K. Hashimoto, M. Okawa, A. Fujishima, Photoelectrochemical reduction of CO_2 at high current densities at *p*-InP electrodes, J. Electrochem. Soc. 145 (1998) L82–L84.
[125] X. Liu, P. Schlexer, J. Xiao, Y. Ji, L. Wang, R.B. Sandberg, M. Tang, K.S. Brown, H. Peng, S. Ringe, C. Hahn, T.F. Jaramillo, J.K. Nørskov, K. Chan, pH effects on the electrochemical reduction of $CO_{(2)}$ towards C2 products on stepped copper, Nat. Commun. 10 (2019) 32.
[126] H. Zhong, K. Fujii, Y. Nakano, F. Jin, Effect of CO_2 bubbling into aqueous solutions used for electrochemical reduction of CO_2 for energy conversion and storage, J. Phys. Chem. C 119 (2015) 55–61.
[127] M. Mikkelsen, M. Jørgensen, F.C. Krebs, The teraton challenge. A review of fixation and transformation of carbon dioxide, Energy Environ. Sci. 3 (2010) 43–81.

[128] J.F. de Brito, A.R. Araujo, K. Rajeshwar, M.V.B. Zanoni, Photoelectrochemical reduction of CO_2 on Cu/Cu_2O films: product distribution and pH effects, Chem. Eng. J. 264 (2015) 302–309.
[129] M. Dunwell, Q. Lu, J.M. Heyes, J. Rosen, J.G. Chen, Y. Yan, F. Jiao, B. Xu, The central role of bicarbonate in the electrochemical reduction of carbon dioxide on gold, J. Am. Chem. Soc. 139 (2017) 3774–3783.
[130] M.R. Singh, E.L. Clark, A.T. Bell, Effects of electrolyte, catalyst, and membrane composition and operating conditions on the performance of solar-driven electrochemical reduction of carbon dioxide, Phys. Chem. Chem. Phys. 17 (2015) 18924–18936.
[131] M. Dunwell, X. Yang, B.P. Setzler, J. Anibal, Y. Yan, B. Xu, Examination of near-electrode concentration gradients and kinetic impacts on the electrochemical reduction of CO_2 using surface-enhanced infrared spectroscopy, ACS Catal. 8 (2018) 3999–4008.
[132] N. Gupta, M. Gattrell, B. MacDougall, Calculation for the cathode surface concentrations in the electrochemical reduction of CO_2 in $KHCO_3$ Solutions, J. Appl. Electrochem. 36 (2006) 161–172.
[133] M.R. Singh, Y. Kwon, Y. Lum, J.W. Ager, A.T. Bell, Hydrolysis of electrolyte cations enhances the electrochemical reduction of CO_2 over Ag and Cu, J. Am. Chem. Soc. 138 (2016) 13006–13012.
[134] E. Pérez-Gallent, G. Marcandalli, M.C. Figueiredo, F. Calle-Vallejo, M.T.M. Koper, Structure- and potential-dependent cation effects on CO reduction at copper single-crystal electrodes, J. Am. Chem. Soc. 139 (2017) 16412–16419.
[135] A.S. Varela, W. Ju, T. Reier, P. Strasser, Tuning the catalytic activity and selectivity of Cu for CO_2 electroreduction in the presence of halides, ACS Catal. 6 (2016) 2136–2144.
[136] M.R. Hasan, S.B. Abd Hamid, W.J. Basirun, S.H. Meriam Suhaimy, A.N. Che Mat, A sol–gel derived, copper-doped, titanium dioxide–reduced graphene oxide nanocomposite electrode for the photoelectrocatalytic reduction of CO_2 to methanol and formic acid, RSC Adv. 5 (2015) 77803–77813.
[137] M. Dilla, A. Mateblowski, S. Ristig, J. Strunk, Photocatalytic CO_2 reduction under continuous flow high-purity conditions: influence of light intensity and H_2O concentration, ChemCatChem 9 (2017) 4345–4352.
[138] J. Gu, A. Wuttig, J.W. Krizan, Y. Hu, Z.M. Detweiler, R.J. Cava, A.B. Bocarsly, Mg-Doped $CuFeO_2$ photocathodes for photoelectrochemical reduction of carbon dioxide, J. Phys. Chem. C 117 (2013) 12415–12422.
[139] H. Peng, J. Lu, C. Wu, Z. Yang, H. Chen, W. Song, P. Li, H. Yin, Co-doped MoS_2 NPs with matched energy band and low overpotential high efficiently convert CO_2 to methanol, Appl. Surf. Sci. 353 (2015) 1003–1012.
[140] N. Sagara, S. Kamimura, T. Tsubota, T. Ohno, Photoelectrochemical CO_2 reduction by a p-type boron-doped g-C_3N_4 electrode under visible light, Appl. Catal. B Environ. 192 (2016) 193–198.
[141] J.S. DuChene, G. Tagliabue, A.J. Welch, W.-H. Cheng, H.A. Atwater, Hot hole collection and photoelectrochemical CO_2 reduction with plasmonic Au/*p*-GaN photocathodes, Nano Lett. 18 (2018) 2545–2550.
[142] Y. Kim, E.B. Creel, E.R. Corson, B.D. McCloskey, J.J. Urban, R. Kostecki, Surface-plasmon-assisted photoelectrochemical reduction of CO_2 and NO_3^- on nanostructured silver electrodes, Adv. Energy Mater. 8 (2018), 1800363.
[143] K.R. Rao, S. Pishgar, J. Strain, B. Kumar, V. Atla, S. Kumari, Joshua M. Spurgeon, Photoelectrochemical reduction of CO_2 to HCOOH on silicon photocathodes with reduced SnO_2 porous nanowire catalysts, J. Mater. Chem. A 6 (2018) 1736–1742.
[144] Q. Shen, Z. Chen, X. Huang, M. Liu, G. Zhao, High-yield and selective photoelectrocatalytic reduction of CO_2 to formate by metallic copper decorated Co_3O_4 nanotube arrays, Environ. Sci. Technol. 49 (2015) 5828–5835.
[145] W. Lu, F. Ju, K. Yao, X. Wei, Photoelectrocatalytic reduction of CO_2 for efficient methanol production: Au nanoparticles as electrocatalysts and light supports, Ind. Eng. Chem. Res. 59 (2020) 4348–4357.
[146] Y. Xu, Y. Jia, Y. Zhang, R. Nie, Z. Zhu, J. Wang, H. Jing, Photoelectrocatalytic reduction of CO_2 to methanol over the multi-functionalized TiO_2 photocathodes, Appl. Catal. B Environ. 205 (2017) 254–261.
[147] D. Guzmán, M. Isaacs, I. Osorio-Román, M. García, J. Astudillo, M. Ohlbaum, Photoelectrochemical reduction of carbon dioxide on quantum-dot-modified electrodes by electric field directed layer-by-layer assembly methodology, ACS Appl. Mater. Interfaces 7 (2015) 19865–19869.
[148] F. Xing, Q. Liu, M. Song, C. Huang, Fluorine modified boron carbon nitride semiconductors for improved photocatalytic CO_2 reduction under visible light, ChemCatChem 10 (2018) 5270–5279.
[149] T. Di, B. Zhu, B. Cheng, J. Yu, J. Xu, A direct Z-scheme g-C_3N_4/SnS_2 photocatalyst with superior visible-light CO_2 reduction performance, J. Catal. 352 (2017) 532–541.
[150] J. Low, L. Zhang, T. Tong, B. Shen, J. Yu, TiO_2/MXene Ti_3C_2 composite with excellent photocatalytic CO_2 reduction activity, J. Catal. 361 (2018) 255–266.
[151] X. Wang, J. He, J. Li, G. Lu, F. Dong, T. Majima, M. Zhu, Immobilizing perovskite $CsPbBr_3$ nanocrystals on Black phosphorus nanosheets for boosting charge separation and photocatalytic CO_2 reduction, Appl. Catal. B Environ. 277 (2020), 119230.
[152] W. Zhu, C. Zhang, Q. Li, L. Xiong, R. Chen, X. Wan, Z. Wang, W. Chen, Z. Deng, Y. Peng, Selective reduction of CO_2 by conductive MOF nanosheets as an efficient co-catalyst under visible light illumination, Appl. Catal. B Environ. 238 (2018) 339–345.
[153] G. Shi, L. Yang, Z. Liu, X. Chen, J. Zhou, Y. Yu, Photocatalytic reduction of CO_2 to CO over copper decorated g-C3N4 nanosheets with enhanced yield and selectivity, Appl. Surf. Sci. 427 (2018) 1165–1173.
[154] P. Yang, Z. Yang, Modulating charge separation and transfer kinetics in carbon nanodots for photoredox catalysis, J. Energy Chem. 50 (2020) 365–377.
[155] Y. Oh, X. Hu, Organic molecules as mediators and catalysts for photocatalytic and electrocatalytic CO_2 reduction, Chem. Soc. Rev. 42 (2013) 2253–2261.
[156] S. Bai, W. Yin, L. Wang, Z. Li, Y. Xiong, Surface and interface design in cocatalysts for photocatalytic water splitting and CO_2 reduction, RSC Adv. 6 (2016) 57446–57463.
[157] Y. Li, W.-N. Wang, Z. Zhan, M.-H. Woo, C.-Y. Wu, P. Biswas, Photocatalytic reduction of CO_2 with H_2O on mesoporous silica supported Cu/TiO_2 catalysts, Appl. Catal. B Environ. 100 (2010) 386–392.
[158] P. Kar, S. Farsinezhad, N. Mahdi, Y. Zhang, U. Obuekwe, H. Sharma, J. Shen, N. Semagina, K. Shankar, Enhanced CH_4 yield by photocatalytic CO_2 reduction using TiO_2 nanotube arrays grafted with Au, Ru, and ZnPd nanoparticles, Nano Res. 9 (2016) 3478–3493.
[159] H. Li, Y. Gao, Z. Xiong, C. Liao, K. Shih, Enhanced selective photocatalytic reduction of CO_2 to CH_4 over plasmonic Au modified g-C_3N_4 photocatalyst under UV–vis light irradiation, Appl. Surf. Sci. 439 (2018) 552–559.
[160] J. Yang, D. Wang, H. Han, C. Li, Roles of cocatalysts in photocatalysis and photoelectrocatalysis, Acc. Chem. Res. 46 (2013) 1900–1909.
[161] W. Ma, M. Xie, S. Xie, L. Wei, Y. Cai, Q. Zhang, Y. Wang, Nickel and indium core-shell co-catalysts loaded silicon nanowire arrays for efficient photoelectrocatalytic reduction of CO_2 to formate, J. Energy Chem. 54 (2021) 422–428.
[162] S. Kaneco, H. Katsumata, T. Suzuki, K. Ohta, Photoelectrocatalytic reduction of CO_2 in LiOH/methanol at metal-modified *p*-InP electrodes, Appl. Catal. B Environ. 64 (2006) 139–145.
[163] R. Hinogami, Y. Nakamura, S. Yae, Y. Nakato, An Approach to Ideal Semiconductor electrodes for efficient photoelectrochemical reduction of carbon dioxide by modification with small metal particles, J. Phys. Chem. B 102 (1998) 974–980.
[164] S. Ikeda, Y. Saito, M. Yoshida, H. Noda, M. Maeda, K. Ito, Photoelectrochemical reduction products of carbon dioxide at metal coated *p*-GaP photocathodes in non-aqueous electrolytes, J. Electroanal. Chem. Interfacial Electrochem. 260 (1989) 335–345.
[165] Y.J. Jang, J.-W. Jang, J. Lee, J.H. Kim, H. Kumagai, J. Lee, T. Minegishi, J. Kubota, K. Domen, J.S. Lee, Selective CO production by Au coupled ZnTe/ZnO in the photoelectrochemical CO_2 reduction system, Energy Environ. Sci. 8 (2015) 3597–3604.
[166] J.L. Gunjakar, I.Y. Kim, J.M. Lee, N.S. Lee, S.J. Hwang, Self-assembly of layered double hydroxide 2D nanoplates with graphene nanosheets: an effective way to improve the photocatalytic activity of 2D nanostructured materials for visible light-induced O_2 generation, Energy Environ. Sci. 6 (2013).
[167] J. Low, J. Yu, M. Jaroniec, S. Wageh, A.A. Al-Ghamdi, Heterojunction photocatalysts, Adv. Mater. 29 (2017), 1601694.
[168] H.R. Kim, A. Razzaq, C.A. Grimes, S.-I. In, Heterojunction *p-n-p* Cu_2O/S-TiO/CuO: synthesis and application to photocatalytic conversion of CO_2 to methane, J. CO_2 Util. 20 (2017) 91–96.
[169] B. Shan, S. Vanka, T.-T. Li, L. Troian-Gautier, M.K. Brennaman, Z. Mi, T.J. Meyer, Binary molecular-semiconductor *p–n* junctions for photoelectrocatalytic CO_2 reduction, Nat. Energy 4 (2019) 290–299.
[170] G. Ghadimkhani, N.R. de Tacconi, W. Chanmanee, C. Janaky, K. Rajeshwar, Efficient solar photoelectrosynthesis of methanol from carbon dioxide using hybrid CuO–Cu_2O semiconductor nanorod arrays, Chem. Commun. 49 (2013) 1297–1299.
[171] A.T. Garcia-Esparza, K. Limkrailassiri, F. Leroy, S. Rasul, W. Yu, L. Lin, K. Takanabe, Photoelectrochemical and electrocatalytic properties of thermally oxidized copper oxide for efficient solar fuel production, J. Mater. Chem. A 2 (2014) 7389–7401.
[172] D.H. Won, C.H. Choi, J. Chung, S.I. Woo, Photoelectrochemical production of formic acid and methanol from carbon dioxide on metal-decorated CuO/Cu_2O-layered thin films under visible light irradiation, Appl. Catal. B Environ. 158–159 (2014) 217–223.
[173] U. Kang, S.K. Choi, D.J. Ham, S.M. Ji, W. Choi, D.S. Han, A. Abdel-Wahab, H. Park, Photosynthesis of formate from CO_2 and water at 1% energy efficiency via copper iron oxide catalysis, Energy Environ. Sci. 8 (2015) 2638–2643.
[174] Y. Xu, S. Wang, J. Yang, B. Han, R. Nie, J. Wang, Y. Dong, X. Yu, J. Wang, H. Jing, Highly efficient photoelectrocatalytic reduction of CO_2 on the Ti_3C_2/g-C_3N_4 heterojunction with rich Ti^{3+} and pyri-N species, J. Mater. Chem. A 6 (2018) 15213–15220.
[175] J. Di, C. Chen, C. Zhu, P. Song, J. Xiong, M. Ji, J. Zhou, Q. Fu, M. Xu, W. Hao, J. Xia, S. Li, H. Li, Z. Liu, Bismuth vacancy-tuned bismuth oxybromide ultrathin nanosheets toward photocatalytic CO_2 reduction, ACS Appl. Mater. Interfaces 11 (2019) 30786–30792.
[176] J. Wu, X. Li, W. Shi, P. Ling, Y. Sun, X. Jiao, S. Gao, L. Liang, J. Xu, W. Yan, C. Wang, Y. Xie, Efficient visible-light-driven CO_2 reduction mediated by defect-engineered BiOBr atomic layers, Angew. Chem. Int. Ed. 130 (2018) 8855–8859.
[177] Y. Wang, P. Han, X. Lv, L. Zhang, G. Zheng, Defect and interface engineering for aqueous electrocatalytic CO_2 reduction, Joule 2 (2018) 2551–2582.
[178] D. Xue, H. Xia, W. Yan, J. Zhang, S. Mu, Defect engineering on carbon-based catalysts for electrocatalytic CO_2 reduction, Nano-Micro Lett. 13 (2020) 5.
[179] Q. Wang, Y. Lei, D. Wang, Y. Li, Defect engineering in earth-abundant electrocatalysts for CO_2 and N_2 reduction, Energy Environ. Sci. 12 (2019) 1730–1750.
[180] J.-Y. Liu, X.-Q. Gong, R. Li, H. Shi, S.B. Cronin, A.N. Alexandrova, (Photo) Electrocatalytic CO_2 reduction at the defective anatase TiO_2 (101) Surface, ACS Catal. 10 (2020) 4048–4058.
[181] X. Ren, Y. Gao, L. Zheng, Z. Wang, P. Wang, Z. Zheng, Y. Liu, H. Cheng, Y. Dai, B. Huang, Oxygen vacancy enhancing CO_2 electrochemical reduction to CO on Ce-doped ZnO catalysts, Surf. Interfaces 23 (2021), 100923.

[182] M. Kong, Y. Li, X. Chen, T. Tian, X. Zhao, Tuning the relative concentration ratio of bulk defects to surface defects in TiO_2 nanocrystals leads to high photocatalytic efficiency, J. Am. Chem. Soc. 133 (2011) 16414–16417.
[183] L.B. Hoch, P. Szymanski, K.K. Ghuman, L. He, K. Liao, Q. Qiao, L.M. Reyes, Y. Zhu, M.A. El-Sayed, C.V. Singh, G.A. Ozin, Carrier dynamics and the role of surface defects: designing a photocatalyst for gas-phase CO_2 reduction, Proc. Natl. Acad. Sci. U.S.A. 113 (2016) E8011.
[184] N. Zhang, C. Gao, Y. Xiong, Defect engineering: a versatile tool for tuning the activation of key molecules in photocatalytic reactions, J. Energy Chem. 37 (2019) 43–57.
[185] H. Yang, Y. Li, D. Zhang, Z. Li, J. Wang, D. Yang, X. Hao, G. Guan, Defect-engineering of tin oxide via (Cu, N) co-doping for electrocatalytic and photocatalytic CO_2 reduction into formate, Chem. Eng. Sci. 227 (2020), 115947.
[186] Y. Zheng, W. Zhang, Y. Li, J. Chen, B. Yu, J. Wang, L. Zhang, J. Zhang, Energy related CO_2 conversion and utilization: advanced materials/nanomaterials, reaction mechanisms and technologies, Nano Energy 40 (2017) 512–539.
[187] B. Han, X. Ou, Z. Deng, Y. Song, C. Tian, H. Deng, Y.-J. Xu, Z. Lin, Nickel Metal–organic framework monolayers for photoreduction of diluted CO_2: metal-node-dependent activity and selectivity, Angew. Chem. Int. Ed. 57 (2018) 16811–16815.
[188] E. Karamian, S. Sharifnia, On the general mechanism of photocatalytic reduction of CO_2, J. CO_2 Util. 16 (2016) 194–203.
[189] Z.-C. Fu, R.-C. Xu, J.T. Moore, F. Liang, X.-C. Nie, C. Mi, J. Mo, Y. Xu, Q.-Q. Xu, Z. Yang, Z.-S. Lin, W.-F. Fu, Highly efficient photocatalytic system constructed from CoP/carbon nanotubes or graphene for visible-light-driven CO_2 reduction, Chem. Eur J. 24 (2018) 4273–4278.
[190] K.-H. Kim, S. Kim, B.C. Moon, J.W. Choi, H.M. Jeong, Y. Kwon, S. Kwon, H.S. Choi, J.K. Kang, Quadruple metal-based layered structure as the photocatalyst for conversion of carbon dioxide into a value added carbon monoxide with high selectivity and efficiency, J. Mater. Chem. A 5 (2017) 8274–8279.
[191] Y. Zhao, Y. Wei, X. Wu, H. Zheng, Z. Zhao, J. Liu, J. Li, Graphene-wrapped Pt/TiO_2 photocatalysts with enhanced photogenerated charges separation and reactant adsorption for high selective photoreduction of CO_2 to CH_4, Appl. Catal. B Environ. 226 (2018) 360–372.
[192] Q. Xu, J. Yu, J. Zhang, J. Zhang, G. Liu, Cubic anatase TiO_2 nanocrystals with enhanced photocatalytic CO_2 reduction activity, Chem. Commun. 51 (2015) 7950–7953.
[193] Z. Xiong, Z. Lei, C.-C. Kuang, X. Chen, B. Gong, Y. Zhao, J. Zhang, C. Zheng, J.C.S. Wu, Selective photocatalytic reduction of CO_2 into CH_4 over Pt-Cu_2O TiO_2 nanocrystals: the interaction between Pt and Cu_2O cocatalysts, Appl. Catal. B Environ. 202 (2017) 695–703.
[194] F. Ye, F. Wang, C. Meng, L. Bai, J. Li, P. Xing, B. Teng, L. Zhao, S. Bai, Crystalline phase engineering on cocatalysts: a promising approach to enhancement on photocatalytic conversion of carbon dioxide to fuels, Appl. Catal. B Environ. 230 (2018) 145–153.
[195] Y. Wang, J. Zhao, Y. Li, C. Wang, Selective photocatalytic CO_2 reduction to CH_4 over Pt/In_2O_3: significant role of hydrogen adatom, Appl. Catal. B Environ. 226 (2018) 544–553.
[196] J.C. Cardoso, S. Stulp, J.F. de Brito, J.B.S. Flor, R.C.G. Frem, M.V.B. Zanoni, MOFs based on ZIF-8 deposited on TiO_2 nanotubes increase the surface adsorption of CO_2 and its photoelectrocatalytic reduction to alcohols in aqueous media, Appl. Catal. B Environ. 225 (2018) 563–573.
[197] Q. Shen, X. Huang, J. Liu, C. Guo, G. Zhao, Biomimetic photoelectrocatalytic conversion of greenhouse gas carbon dioxide: two-electron reduction for efficient formate production, Appl. Catal. B Environ. 201 (2017) 70–76.
[198] X. Huang, Q. Shen, J. Liu, N. Yang, G. Zhao, A CO_2 adsorption-enhanced semiconductor/metal-complex hybrid photoelectrocatalytic interface for efficient formate production, Energy Environ. Sci. 9 (2016) 3161–3171.
[199] L. Wang, W. Chen, D. Zhang, Y. Du, R. Amal, S. Qiao, J. Wu, Z. Yin, Surface strategies for catalytic CO_2 reduction: from two-dimensional materials to nanoclusters to single atoms, Chem. Soc. Rev. 48 (2019) 5310–5349.
[200] Y. Chen, Y. Huang, T. Cheng, W.A. Goddard, Identifying active sites for CO_2 reduction on dealloyed gold surfaces by combining machine learning with multiscale simulations, J. Am. Chem. Soc. 141 (2019) 11651–11657.
[201] S. Back, M.S. Yeom, Y. Jung, Active sites of Au and Ag nanoparticle catalysts for CO_2 electroreduction to CO, ACS Catal. 5 (2015) 5089–5096.
[202] S. Kattel, P.J. Ramírez, J.G. Chen, J.A. Rodriguez, P. Liu, Active sites for CO_2 hydrogenation to methanol on Cu/ZnO catalysts, Science 355 (2017) 1296.
[203] Q. Lang, Y. Yang, Y. Zhu, W. Hu, W. Jiang, S. Zhong, P. Gong, B. Teng, L. Zhao, S. Bai, High-index facet engineering of PtCu cocatalysts for superior photocatalytic reduction of CO_2 to CH_4, J. Mater. Chem. A 5 (2017) 6686–6694.
[204] L. Lu, S. Wang, C. Zhou, Z. Shi, H. Zhu, Z. Xin, X. Wang, S. Yan, Z. Zou, Surface chemistry imposes selective reduction of CO_2 to CO over Ta_3N_5/$LaTiO_2N$ photocatalyst, J. Mater. Chem. A 6 (2018) 14838–14846.
[205] W. Tu, Y. Li, L. Kuai, Y. Zhou, Q. Xu, H. Li, X. Wang, M. Xiao, Z. Zou, Construction of unique two-dimensional MoS_2–TiO_2 hybrid nanojunctions: MoS_2 as a promising cost-effective cocatalyst toward improved photocatalytic reduction of CO_2 to methanol, Nanoscale 9 (2017) 9065–9070.
[206] K. Liu, X. Li, L. Liang, J. Wu, X. Jiao, J. Xu, Y. Sun, Y. Xie, Ni-doped $ZnCo_2O_4$ atomic layers to boost the selectivity in solar-driven reduction of CO_2, Nano Res. 11 (2018) 2897–2908.
[207] H. Zhang, T. Wang, J. Wang, H. Liu, T.D. Dao, M. Li, G. Liu, X. Meng, K. Chang, L. Shi, T. Nagao, J. Ye, Surface-plasmon-enhanced photodriven CO_2 reduction catalyzed by metal–organic-framework-derived iron nanoparticles encapsulated by ultrathin carbon layers, Adv. Mater. 28 (2016) 3703–3710.
[208] S. Sorcar, J. Thompson, Y. Hwang, Y.H. Park, T. Majima, C.A. Grimes, J.R. Durrant, S.-I In, High-rate solar-light photoconversion of CO_2 to fuel: controllable transformation from C_1 to C_2 products, Energy Environ. Sci. 11 (2018) 3183–3193.
[209] M.T. Galante, P.V.B. Santiago, V.Y. Yukuhiro, L.A. Silva, N.A. Dos Reis, C.T. Pires, N.G. Macedo, L.S. Costa, P.S. Fernandez, C. Longo, Aminopolysiloxane as Cu_2O photocathode overlayer: photocorrosion inhibitor and low overpotential CO_2-to-formate selectivity promoter, ChemCatChem 13 (2021) 859–863.
[210] K.M.R. Karim, M. Tarek, S.M. Sarkar, R. Mouras, H.R. Ong, H. Abdullah, C.K. Cheng, M.M.R. Khan, Photoelectrocatalytic reduction of CO_2 to methanol over $CuFe_2O_4$@PANI photocathode, Int. J. Hydrogen Energy (2020), https://doi.org/10.1016/j.ijhydene.2020.02.195.
[211] J. Wu, X. Han, D. Li, B.E. Logan, J. Liu, Z. Zhang, Y. Feng, Efficient CO_2 conversion to formic acid in a novel microbial photoelectrochemical cell using a visible-light responsive Co_3O_4 nanorod-arrayed photocathode, Appl. Catal. B Environ. 276 (2020), 119102.
[212] S. Chu, P. Ou, Y. Pan, D. Liang, H. Zhang, J. Song, Z. Mi, Efficient Photoelectrochemical Conversion of CO2 to Syngas by Photocathode Engineering, Green Energy Environ, 2020, https://doi.org/10.1016/j.gee.2020.11.015.
[213] J.S. DuChene, G. Tagliabue, A.J. Welch, X. Li, W.-H. Cheng, H.A. Atwater, Optical excitation of a nanoparticle Cu/*p*-NiO photocathode improves reaction selectivity for CO_2 reduction in aqueous electrolytes, Nano Lett. 20 (2020) 2348–2358.
[214] H. Zhang, Y. Chen, H. Wang, H. Wang, W. Ma, X. Zong, C. Li, Carbon encapsulation of organic–inorganic hybrid perovskite toward efficient and stable photo-electrochemical carbon dioxide reduction, Adv. Energy Mater. 10 (2020), 2002105.
[215] S.-H. Oh, H.-Y. Kang, W.-H. Joo, Y.-C. Joo, Photoelectrochemical CO_2 reduction via Cu_2O/$CuFeO_2$ hierarchical nanorods photocatalyst, ChemCatChem 12 (2020) 5185–5191.
[216] D. Fu, J. Tourneur, B. Fabre, G. Loget, Y. Lou, F. Geneste, S. Ababou-Girard, C. Mériadec, Bismuth-decorated silicon photocathodes for CO_2-to-formate solar-driven conversion, ChemCatChem 12 (2020) 5819–5825.
[217] K. Irikura, J.A.L. Perini, J.B.S. Flor, R.C.G. Frem, M.V.B. Zanoni, Direct synthesis of $Ru_3(BTC)_2$ metal-organic framework on a Ti/TiO_2NT platform for improved performance in the photoelectroreduction of CO_2, J. CO2 Util. 43 (2021), 101364.
[218] L. Lu, Z. Li, X. Chen, H. Wang, S. Dai, X. Pan, Z.J. Ren, J. Gu, Spontaneous solar syngas production from CO_2 driven by energetically favorable wastewater microbial anodes, Joule 4 (2020) 2149–2161.
[219] J.A.L. Perini, L.D.M. Torquato, K. Irikura, M.V.B. Zanoni, Ag/polydopamine-modified Ti/TiO_2 nanotube arrays: a platform for enhanced CO_2 photoelectroreduction to methanol, J. CO_2 Util. 34 (2019) 596–605.
[220] S. Ikeda, S. Fujikawa, T. Harada, T.H. Nguyen, S. Nakanishi, T. Takayama, A. Iwase, A. Kudo, Photocathode characteristics of a spray-deposited Cu_2ZnGeS_4 thin film for CO_2 reduction in a CO_2-saturated aqueous solution, ACS Appl. Energy Mater. 2 (2019) 6911–6918.
[221] T.-T. Li, B. Shan, T.J. Meyer, Stable molecular photocathode for solar-driven CO_2 reduction in aqueous solutions, ACS Energy Lett. 4 (2019) 629–636.
[222] C. Li, T. Wang, B. Liu, M. Chen, A. Li, G. Zhang, M. Du, H. Wang, S.F. Liu, J. Gong, Photoelectrochemical CO_2 reduction to adjustable syngas on grain-boundary-mediated a-Si/TiO_2/Au photocathodes with low onset potentials, Energy Environ. Sci. 12 (2019) 923–928.
[223] J.W. Gurudayal, J. Beeman, H. Bullock, J. Wang, C. Eichhorn, A. Towle, F.M. Javey, N. Toma, J.W. Mathews, Ager, Si photocathode with Ag-supported dendritic Cu catalyst for CO_2 reduction, Energy Environ. Sci. 12 (2019) 1068–1077.
[224] J. Huang, B. Xu, L. Tian, P.B. Pati, A.S. Etman, J. Sun, L. Hammarström, H. Tian, A heavy metal-free $CuInS_2$ quantum dot sensitized NiO photocathode with a Re molecular catalyst for photoelectrochemical CO_2 reduction, Chem. Commun. 55 (2019) 7918–7921.
[225] K.M. Rezaul Karim, H.R. Ong, H. Abdullah, A. Yousuf, C.K. Cheng, M.M. Rahman Khan, Photoelectrochemical reduction of carbon dioxide to methanol on *p*-type $CuFe_2O_4$ under visible light irradiation, Int. J. Hydrogen Energy 43 (2018) 18185–18193.
[226] K. Lee, S. Lee, H. Cho, S. Jeong, W.D. Kim, S. Lee, D.C. Lee, Cu^+-incorporated TiO_2 overlayer on Cu_2O nanowire photocathodes for enhanced photoelectrochemical conversion of CO_2 to methanol, J. Energy Chem. 27 (2018) 264–270.
[227] X. Yang, E.A. Fugate, Y. Mueanngern, L.R. Baker, Photoelectrochemical CO_2 reduction to acetate on iron–copper oxide catalysts, ACS Catal. 7 (2017) 177–180.
[228] Q. Shen, J. Ma, X. Huang, N. Yang, G. Zhao, Enhanced carbon dioxide conversion to formate on a multi-functional synergistic photoelectrocatalytic interface, Appl. Catal. B Environ. 219 (2017) 45–52.
[229] J.T. Song, H. Ryoo, M. Cho, J. Kim, J.-G. Kim, S.-Y. Chung, J. Oh, Nanoporous Au thin films on Si photoelectrodes for selective and efficient photoelectrochemical CO_2 reduction, Adv. Energy Mater. 7 (2017), 1601103.
[230] Q. Kong, D. Kim, C. Liu, Y. Yu, Y. Su, Y. Li, P. Yang, Directed assembly of nanoparticle catalysts on nanowire photoelectrodes for photoelectrochemical CO_2 reduction, Nano Lett. 16 (2016) 5675–5680.
[231] K. Kobayashi, S.N. Lou, Y. Takatsuji, T. Haruyama, Y. Shimizu, T. Ohno, Photoelectrochemical reduction of CO_2 using a TiO_2 photoanode and a gas diffusion electrode modified with a metal phthalocyanine catalyst, Electrochim. Acta 338 (2020), 135805.
[232] D. Pan, X. Ye, Y. Cao, S. Zhu, X. Chen, M. Chen, D. Zhang, G. Li, Photoanode driven photoelectrocatalytic system for CO_2 reduction to formic acid by using CoO_x cathode, Appl. Surf. Sci. 511 (2020), 145497.

[233] B. Bian, L. Shi, K.P. Katuri, J. Xu, P. Wang, P.E. Saikaly, Efficient solar-to-acetate conversion from CO_2 through microbial electrosynthesis coupled with stable photoanode, Appl. Energy 278 (2020), 115684.
[234] S. Xiao, Z. Li, Q. Fu, Y. Li, J. Li, L. Zhang, Q. Liao, X. Zhu, Hybrid microbial photoelectrochemical system reduces CO_2 to CH_4 with 1.28% solar energy conversion efficiency, Chem. Eng. J. 390 (2020), 124530.
[235] Y. Ma, Y. Fang, X. Fu, X. Wang, Photoelectrochemical conversion of CO_2 into HCOOH using a polymeric carbon nitride photoanode and Cu cathode, Sustain. Energy Fuels 4 (2020) 5812–5817.
[236] S. Castro, J. Albo, A. Irabien, Continuous conversion of CO_2 to alcohols in a TiO_2 photoanode-driven photoelectrochemical system, J. Chem. Technol. Biotechnol. 95 (2020) 1876–1882.
[237] S. Ajmal, Y. Yang, K. Li, M.A. Tahir, Y. Liu, T. Wang, A.-U.-R. Bacha, Y. Feng, Y. Deng, L. Zhang, Zinc-Modified Copper catalyst for efficient (photo-) electrochemical CO_2 reduction with high selectivity of HCOOH production, J. Phys. Chem. C 123 (2019) 11555–11563.
[238] L.-X. Liu, J. Fu, L.-P. Jiang, J.-R. Zhang, W. Zhu, Y. Lin, Highly efficient photoelectrochemical reduction of CO_2 at low external voltage using 3D Co-Pi/$BiVO_4$/SnO_2 nanosheet array photoanodes, ACS Appl. Mater. Interfaces 11 (2019) 26024–26031.
[239] Z. Li, H. Cheng, Y. Li, W. Zhang, Y. Yu, H_2O_2 treated CdS with enhanced activity and improved stability by a weak negative bias for CO_2 photoelectrocatalytic reduction, ACS Sustain. Chem. Eng. 7 (2019) 4325–4334.
[240] X. Chang, T. Wang, Z.-J. Zhao, P. Yang, J. Greeley, R. Mu, G. Zhang, Z. Gong, Z. Luo, J. Chen, Y. Cui, G.A. Ozin, J. Gong, Tuning Cu/Cu_2O interfaces for the reduction of carbon dioxide to methanol in aqueous solutions, Angew. Chem. Int. Ed. 57 (2018) 15415–15419.
[241] W. Liu, Y. Yang, F. Zhan, D. Li, Y. Li, X. Tang, W. Li, J. Li, Ultrafast fabrication of nanostructure WO_3 photoanodes by hybrid microwave annealing with enhanced photoelectrochemical and photoelectrocatalytic activities, Int. J. Hydrogen Energy 43 (2018) 8770–8778.
[242] K.P. Sokol, W.E. Robinson, A.R. Oliveira, J. Warnan, M.M. Nowaczyk, A. Ruff, I.A.C. Pereira, E. Reisner, Photoreduction of CO_2 with a formate dehydrogenase driven by photosystem II using a semi-artificial Z-scheme architecture, J. Am. Chem. Soc. 140 (2018) 16418–16422.
[243] Y. Yang, F. Zhan, H. Li, W. Liu, S. Yu, In situ Sn-doped WO_3 films with enhanced photoelectrochemical performance for reducing CO_2 into formic acid, J. Solid State Electrochem. 21 (2017) 2231–2240.
[244] F. Zhan, W. Liu, W. Li, J. Li, Y. Yang, Q. Liu, Y. Li, X. Tang, Boric acid assisted synthesis of WO_3 nanostructures with highly reactive (002) facet and enhanced photoelectrocatalytic activity, J. Mater. Sci. Mater. Electron. 28 (2017) 13836–13845.
[245] S. Aoi, K. Mase, K. Ohkubo, T. Suenobu, S. Fukuzumi, Selective CO production in photoelectrochemical reduction of CO_2 with a cobalt chlorin complex adsorbed on multiwalled carbon nanotubes in water, ACS Energy Lett. 2 (2017) 532–536.
[246] X. Zhou, R. Liu, K. Sun, Y. Chen, E. Verlage, S.A. Francis, N.S. Lewis, C. Xiang, Solar-driven reduction of 1 atm of CO_2 to formate at 10% energy-conversion efficiency by use of a TiO_2-protected III–V tandem photoanode in conjunction with a bipolar membrane and a Pd/C cathode, ACS Energy Lett. 1 (2016) 764–770.
[247] S.Y. Lee, S.Y. Lim, D. Seo, J.-Y. Lee, T.D. Chung, Light-driven highly selective conversion of CO_2 to formate by electrosynthesized enzyme/cofactor thin film electrode, Adv. Energy Mater. 6 (2016), 1502207.
[248] M. Li, P. Li, K. Chang, H. Liu, X. Hai, H. Zhang, J. Ye, Design of a photoelectrochemical device for the selective conversion of aqueous CO_2 to CO: using mesoporous palladium–copper bimetallic cathode and hierarchical ZnO-based nanowire array photoanode, Chem. Commun. 52 (2016) 8235–8238.
[249] H. Jun, S. Choi, J.B. Lee, Y.S. Nam, Plasmonic heterostructure functionalized with a carbene-linked molecular catalyst for sustainable and selective carbon dioxide reduction, ACS Appl. Mater. Interfaces 12 (2020) 33817–33826.
[250] Y. Dong, R. Nie, J. Wang, X. Yu, P. Tu, J. Chen, H. Jing, Photoelectrocatalytic CO_2 reduction based on metalloporphyrin-modified TiO_2 photocathode, Chin. J. Catal. 40 (2019) 1222–1230.
[251] R. Nie, W. Ma, Y. Dong, Y. Xu, J. Wang, J. Wang, H. Jing, Artificial photosynthesis of methanol by Mn:CdS and CdSeTe quantum dot cosensitized titania photocathode in imine-based ionic liquid aqueous solution, ChemCatChem 10 (2018) 3342–3350.
[252] S.K. Kuk, R.K. Singh, D.H. Nam, R. Singh, J.-K. Lee, C.B. Park, Photoelectrochemical reduction of carbon dioxide to methanol through a highly efficient enzyme cascade, Angew. Chem. Int. Ed. 56 (2017) 3827–3832.
[253] E.J. Son, J.W. Ko, S.K. Kuk, H. Choe, S. Lee, J.H. Kim, D.H. Nam, G.M. Ryu, Y.H. Kim, C.B. Park, Sunlight-assisted, biocatalytic formate synthesis from CO_2 and water using silicon-based photoelectrochemical cells, Chem. Commun. 52 (2016) 9723–9726.
[254] B. Weng, W. Wei, Yiliguma, H. Wu, A.M. Alenizi, G. Zheng, Bifunctional CoP and CoN porous nanocatalysts derived from ZIF-67 in situ grown on nanowire photoelectrodes for efficient photoelectrochemical water splitting and CO_2 reduction, J. Mater. Chem. A 4 (2016) 15353–15360.
[255] J. Wang, Y. Wei, B. Yang, B. Wang, J. Chen, H. Jing, In situ grown heterojunction of Bi_2WO_6/BiOCl for efficient photoelectrocatalytic CO_2 reduction, J. Catal. 377 (2019) 209–217.
[256] Y.J. Jang, I. Jeong, J. Lee, J. Lee, M.J. Ko, J.S. Lee, Unbiased sunlight-driven artificial photosynthesis of carbon monoxide from CO_2 Using a ZnTe-Based photocathode and a perovskite solar cell in tandem, ACS Nano 10 (2016) 6980–6987.
[257] Y. Wang, S. Fan, B. AlOtaibi, Y. Wang, L. Li, Z. Mi, A monolithically integrated gallium nitride nanowire/silicon solar cell photocathode for selective carbon dioxide reduction to methane, Chem. Eur J. 22 (2016) 8809–8813.